UNIVERSITY OF MANITOBA

An Investigation Into the Movement of Alluvial Shale Gravels in the Riding Mountain Area of Manitoba

by Eric-L. Blais

A Thesis Submitted to the Faculty of Graduate Studies in Partial Fulfillment of the Requirements for the Degree of Master of Arts.

Department of Geography

Winnipeg, Manitoba

January, 1980

AN INVESTIGATION INTO THE MOVEMENT OF ALLUVIAL SHALE GRAVELS IN THE RIDING MOUNTAIN AREA OF MANITOBA

BY

ERIC-LORNE BLAIS

A thesis submitted to the Faculty of Graduate Studies of the University of Manitoba in partial fulfillment of the requirements of the degree of

MASTER OF ARTS

ABSTRACT

This study attempts to establish the regional fluvial transport frequency for the shale bedded streams draining the eastern Riding Mountain escarpment by determining the individual transport frequencies for three representative streams found in the region.

Bedload sampling at seventeen sites along these streams provided the grain size distributions essential for the application of a critical erosion velocity formula and established the typical shape of shale particles. Both field and laboratory observations failed to provide conclusive evidence of either the rate or terminal grade of the weathering process, although hydration weathering was found to be predominant.

Flume experiments established the critical erosion velocity formula for shale as $V_{mc} = 0.29\ D_s^{\cdot 50}$, where D_s was defined as the median size of sieved sediment. This formula was utlimately converted so that nominal diameter values could be used and the function became $V_{mc} = 0.34\ D_s^{\cdot 50}$. Velocity in both cases was in m/s. It is believed that the shape of the shale particles compensates for the effect of low specific gravity and causes the required velocities to be similar to those derived by flume experiments employing spheroidal material of higher specific gravity.

Surveys conducted at each site provided the remaining data required to calculate the critical discharges for one site on each stream. The return periods of these discharges were then read from a regional flood frequency curve constructed from the discharge records of three gauged streams found within the study area. The return period for floods capable of causing complete bed mobilization in the Riding Mountain area was found to be 1.3 years.

ACKNOWLEDGEMENTS

The author would like to gratefully acknowledge the time and effort of L. P. Stene and the other members of the examining committee in reading and providing editorial comment on this dissertation. For stimulating an interest in fluial geomorphology and specifically the Riding Mountain area I am indebted to R. A. McGinn. Particular gratitude is expressed to Luis Magalhaes and the Department of Civil Engineering for the use of that department's hydraulics laboratory.

I am forever indebted to Mari Canton for her assistance during the course of field studies and in the writing of this thesis. Moreover, her never ending support and encouragement have to a large extent allowed the successful completion of this work.

I would further like to thank Walter Blais for his companionship during field investigations.

This thesis is dedicated to my parents, Leo and Esther Blais in recognition of a lifetime of support and encouragement.

TABLE OF CONTENTS

LIST OF TABLES

LIST OF FIGURES

LIST OF PLATES

CHAPTER 1

A GENERAL INTRODUCTION TO THE STUDY

1.1 Introduction

The objective of this thesis is to examine the fluvial transport of shale gravels so that the frequency of transport within the small watersheds draining the eastern slopes of Riding Mountain can be determined. As such, it is an attempt to evaluate the effect of shape on the critical erosion velocity for non-spherical gravel.

Interest in the Riding Mountain watershed was promoted by three main factors:

i) These watersheds have a documented history of severe erosional and depositional problems, which is indicative of active bedload transport.

ii) The area's homogeneity with respect to physiography, geology, vegetation, soils and climate allows the use of a regional approach.

iii) The hydrologic and meteorologic data available for this area are not only adequate for this study, but surpasses the data available from other parts of the province.

1.2 Geology and Physiography of the Riding Mountain Area

MacKay and Stanton (1964) subdivided the Manitoba Escarpment watersheds into three physiographic regions; the upper catchment area, the escarpment slope and the alluvial apron. The upper catchment area is a relatively flat plateau elevated about 300 meters above the

Manitoba Lake Plain. Maximum elevations of 730 meters occur in the northern watersheds, with slightly lower maximum values in the south. From the plateau, elevations decrease rapidly towards the east as much as 400 meters in 6.9 kilometers. The streams in this region, the escarpment slope, assume a mountainous character as they flow swiftly through V-shaped valleys up to 150 meters in depth. Downstream gradients decrease as streams emerge from the valleys onto the alluvial apron composed of Holocene alluvial sediments (Figure 1). Glacial deposits cover most of the bedrock formations in the watersheds. Shale beds of upper Cretaceous age underly the glacial drift and form the bedrock exposures occurring in the valleys of the main water courses. The phases of the Riding Mountain formation, the Millwood and the Odanah, dominate in these exposed bedrock areas. The Odanah phase is composed of light grey, hard siliceous shale and is the principal stream bedload material. The Millwood phase, a soft greenish shale is found only in the most downstream sections of the watercourses. Alluvial deposits composed of shale fragments, occur in terraces in the lower portion of the creek valleys and as fan or apron deposits at the base of the escarpment.

1.3 The Study Area

The study area of 500 square kilometers lies east of the Riding Mountain escarpment plateau, in a strip extending between the towns of Eden and McCreary (Figure 2). Seventeen sites along three streams within this area were selected for detailed examination (Figure 3). Sites were distributed from the farthest accessible location upstream, to the point along the stream channel where sediment transport became negligible.

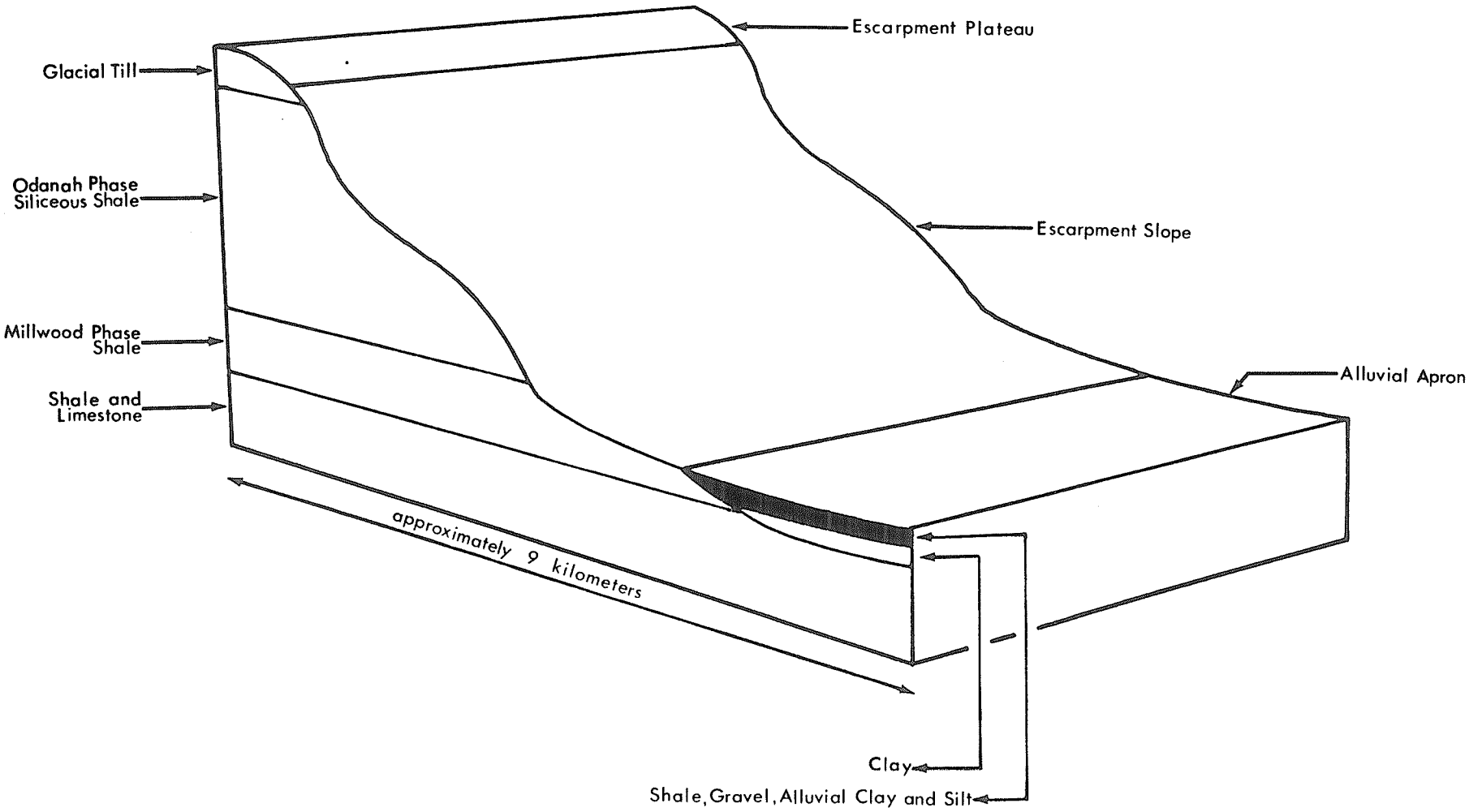
ESCARPMENT CROSS-SECTION
Escarpment Plateau
Glacial Till
Odanah Phase
Siliceous Shale
Escarpment Slope
Millwood Phase
Shale
Alluvial Apron
Shale and
Limestone
approximately 9 kilometers
Clay
Shale, Gravel, Alluvial Clay and Silt

Figure 1.

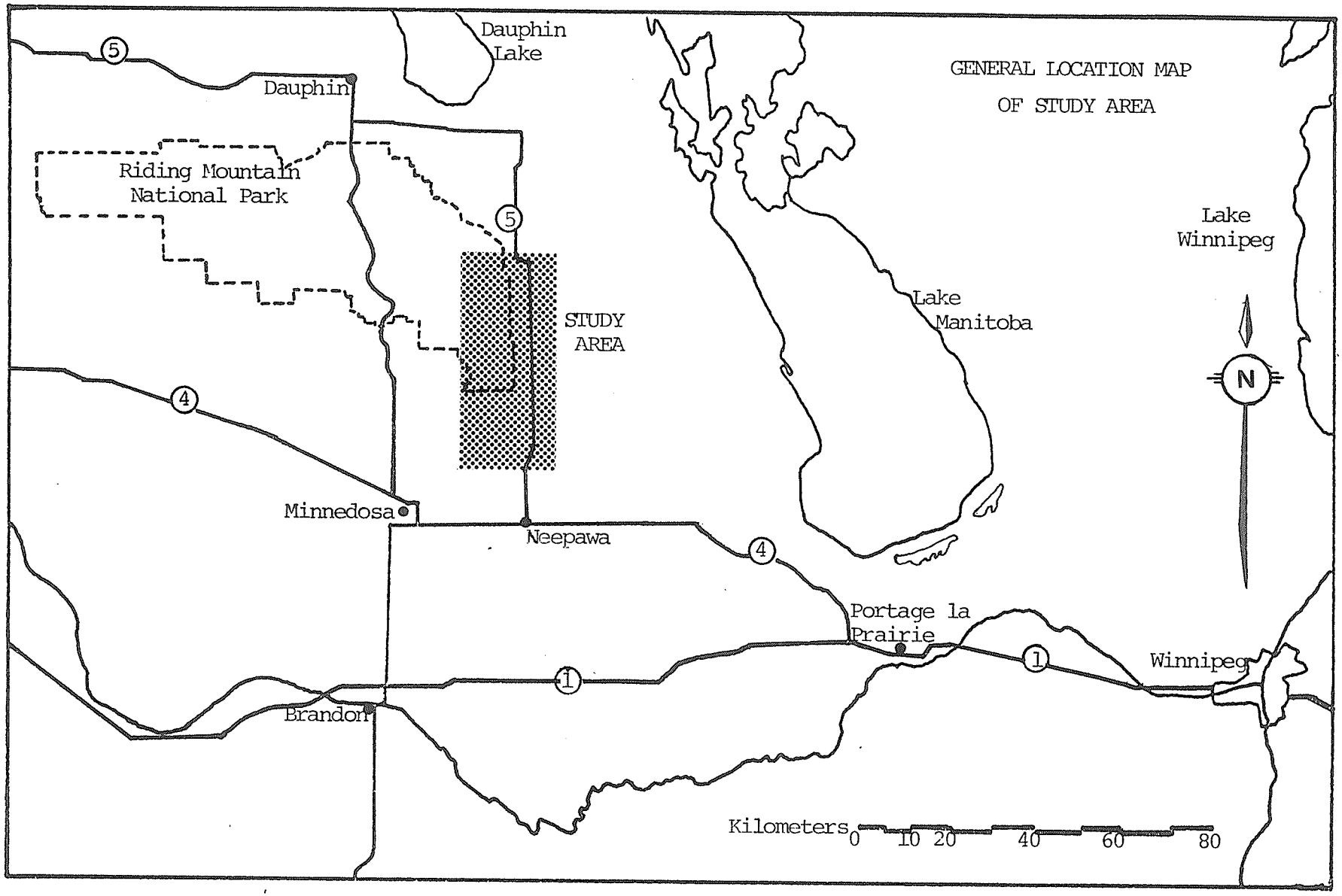
GENERAL LOCATION MAP
OF STUDY AREA
Dauphin Lake
Dauphin
Riding Mountain National Park
STUDY AREA
Lake Manitoba
Lake Winnipeg
N
Minnedosa
Neepawa
Portage la Prairie
Winnipeg
Brandon
5
4
1
Kilometers
0 10 20 40 60 80

Figure 2.

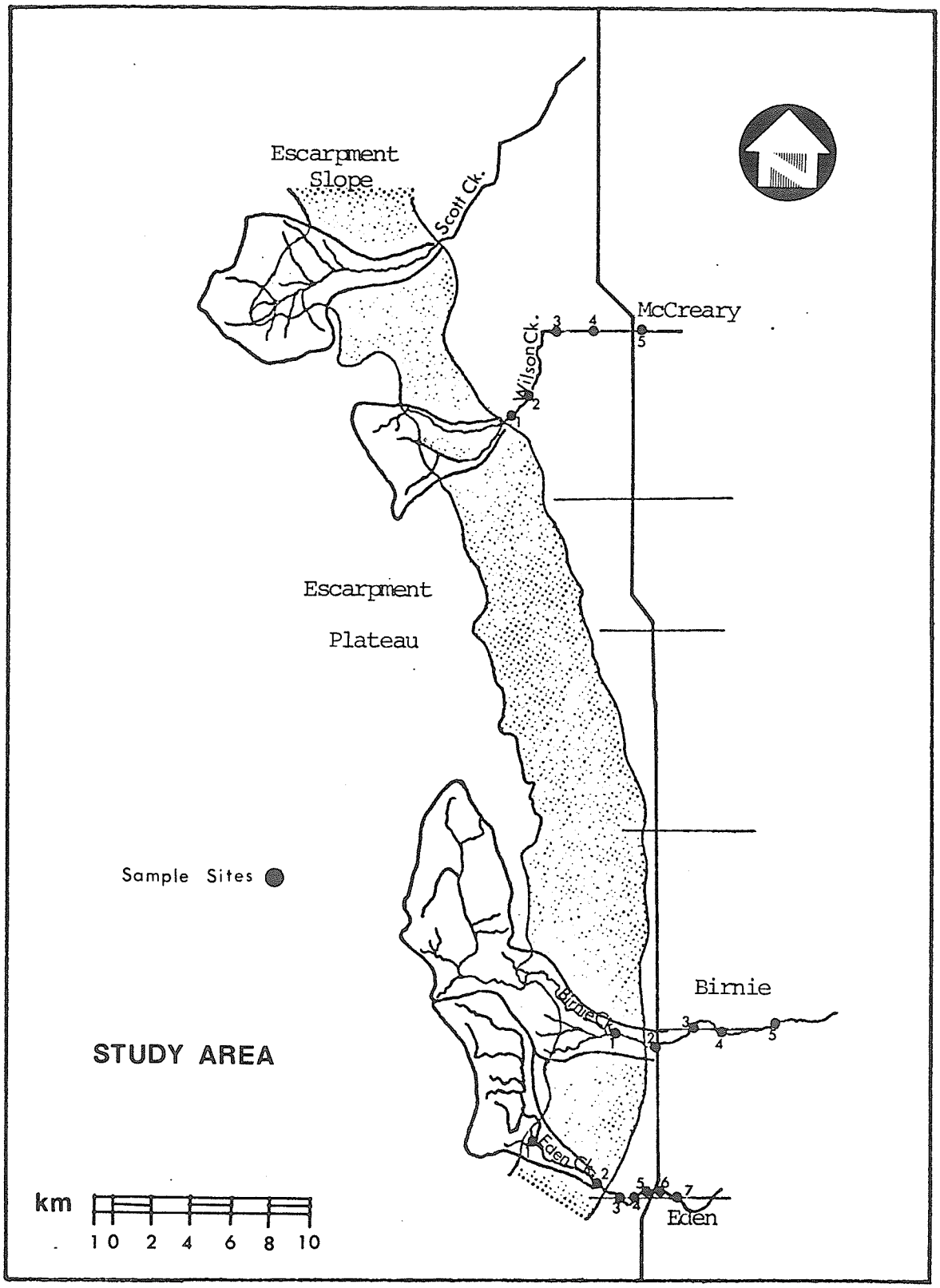
Escarpment
Slope
Scott Ck.
McCreary
Wilson Ck.
1
2
3
4
5
Escarpment
Plateau
Sample Sites
STUDY AREA
Birnie
Birnie Ck.
Eden Ck.
Eden
km
1 0 2 4 6 8 10

Figure 3.

1.4 The Problem of Predicting Sediment Transport

Since the 1700's research into fluvial erosion has focused upon the concept of initial or incipient particle motion. Incipient particle motion occurs when the shear stress associated with stream flow over the bed attains or exceeds a critical value (Simons and Senturk, 1977, p. 399). Simply stated, a threshold exists where the forces promoting movement overcome the specific particle's resistance to movement.

Some researchers have employed a theoretical approach in an attempt to analyze and balance the dynamic forces promoting movement to the resistance forces opposing it, to determine when resistance is overcome and particles begin to move. This approach utilizes a theoretical model to analyze the magnitude of the component forces and is the basis for critical tractive force formulae used by researchers in fluvial hydraulics.

The empirical approach, on the other hand, develops formulae from observations of the initiation of particle motion under natural or laboratory conditions and measurement of discernable parameters. These formulae relate particle size to either the velocity or shear stress required to initiate movement.

1.5 Application of a Regional Approach to Determine the Frequency of Sediment Movement

Fluvial sediment transport is a complex phenomenon affected by many interrelated factors. The main factors which must be examined to achieve an adequate understanding of this process for any particular area are:

i) the sediment characteristics;

ii) the stream flow characteristics;

iii) stream channel morphometry.

For the purposes of this study, sediment characteristics were determined by sampling and triaxial measurement of the bed load material. It was believed that the weathering of shale contributes to the size and shape of the bed material. This process was therefore examined in the field to resolve whether there was a significant decrease in particle size over the field season. The controlled laboratory weathering of a bedload cobble provided additional information on this process.

A regional flood frequency analysis allowed the frequency and magnitude of stream flows for each of the study streams to be determined. Surveys at each of the bedload sampling sites provided the morphometric measurements required to apply flow equations. Finally, flume studies were used to establish the relationship between shale particle size and the flow velocity required to initiate transport. The results of this investigation were compared to data generated by other studies employing spheroidal material to ascertain the effect of shape on the particle entrainment process.

The data provided by these investigations were then employed in a stepwise process, by which the representative fluvial transport frequency for the watersheds of eastern Riding Mountain was determined.

1.6 Summary

The chapters which follow, systematically present the background, methodologies, and results of the study undertaken to evaluate the frequency with which these shale gravels move. The second chapter examines the concept of incipient particle motion, both in terms of the predominant schools of thought and the hydrodynamic explanation for this phenomenon. Chapter three describes the techniques used in:

i) sampling;

ii) weathering experiments;

iii) flood frequency analysis;

iv) surveying of the stream channel;

v) flume experiments.

The results of the sampling and the weathering experiments are also presented in this chapter. Chapter four completes the presentation of data from the studies undertaken along with the stepwise procedure employed to calculate sediment transport frequencies. The final chapter briefly summarizes the study and discusses the major findings and conclusions.

CHAPTER 2

INCIPIENT PARTICLE MOTION RESEARCH

2.1 Introduction

Incipient particle motion is a complex phenomenon which has been analysed in the past using both theoretical and empirical approaches. The theoretical approach attempts to analyze the forces causing a particle to move, but the complexity of the phenomenon limits its applicability when dealing with sediments whose physical characteristics are not easily modelled (e.g. non-spheroidal grains). The empirical approach, on the other hand, involves observation of the phenomenon to derive particle entrainment formulae and, as such, is more versatile. Neither approach, however, clearly explains the physical reasoning for particle motion, as each is only intended for purposes of predicting particle movement. It is therefore imperative that the component forces and the fluid dynamics behind these factors be examined before there can be a discussion of previous research on the topic.

2.2 The Generalized Model of Fluid Forces

Any object submerged in a moving fluid is subject to forces acting both parallel and normal to the flow. The total drag force acting in the direction of flow is the sum of two constituent forces; skin drag and form drag (Shapiro, 1961, p. 81). Skin drag is the force exerted by the fluid as it shears upon itself to maintain motion and as such, is related to the fluid's viscosity, or internal resistance to shear. The pressure field surrounding the object is responsible for

both form drag and a lift force. The pressure field is explained by the Bernoulli principle which states: "Fluid deceleration is accompanied by a rise in pressure along the streamline; conversely, there must be a decrease in pressure along an accelerating streamline" (Shapiro, 1961, p. 141). Therefore, changes in fluid velocity as it passes over and around the object will result in a pressure field developing upon the object's surface. If the pressure on the lee side is less than on the front of the object, form drag is said to exist. Similarly, if the pressure over the upper surface is less than on the bottom a lifting force will result.

2.3 Fluid Dynamics of Drag

An explanation of the fluid dynamics responsible for the generation of lift and drag forces is necessary before the variations in the strength of these forces can be understood. Both the forces governing fluid motion and the forces exerted upon a solid object must be considered to understand the interrelationship between flow and the initiation of particle motion. As such, this section will examine incipient particle motion from a theoretical standpoint and will employ simple models to explain the fluid dynamics at various flow regimes.

It is useful when attempting to visualize the movement of water to imagine it as composed of many separate particles of fluid. The motion of a fluid particle under any flow condition is governed by a balance between the net pressure force, net viscous force and the inertial force. The net pressure force is the force exerted on the fluid particle due to the normal stress or pressure distribution on that particle. Net viscous force is the result of viscous friction and the inertial force is the fluid's inertial resistance to acceleration

or deceleration (Shapiro, 1961, pp.47-55). Similarly, the movement of a solid particle immersed in a fluid will be controlled by the normal forces (pressure) and tangential forces (viscous friction) exerted by the fluid on the solid's surface. The inertial force, in this case, is the particle's inertial resistance to acceleration or deceleration (Shapiro, 1961, p. 80) which is a function of the particle's weight and gravitational attraction.

Fluid motion under laminar flow conditions (very low Reynold's numbers) is governed by a rather static balance between pressure and viscous forces, with inertial forces being negligible. Under these conditions when a viscous fluid, such as water, encounters a solid particle the pressure over the grain's surface will be highest at the front (nose) of the particle and will drop towards the tail (Figure 4). The boundary layer fluid will be pushed to the lee of the particle by this falling pressure gradient and no turbulence will occur (i.e. no pressure drag). The strength of the drag force (viscous or skin drag) developed will be proportional to the surface area over which the viscous stresses act (Shapiro, 1961, p. 160).

At very high Reynold's numbers (turbulent flow), viscous forces are important only in the very thin boundary layer close to the grain's surface with the remainder of the flow behaving in an essentially non-viscous manner (Shapiro, 1961, p. 143). The pressure distribution impressed upon the boundary layer fluid and the grain's surface is established by this main body of 'non-viscous' fluid. The fluid particles in the slow-moving boundary move according to the forces produced by this pressure distribution (Shapiro, 1961, p. 143).

The pressure distribution established can be accounted for by the Bernoulli principle. The velocity of flow is reduced to zero at the

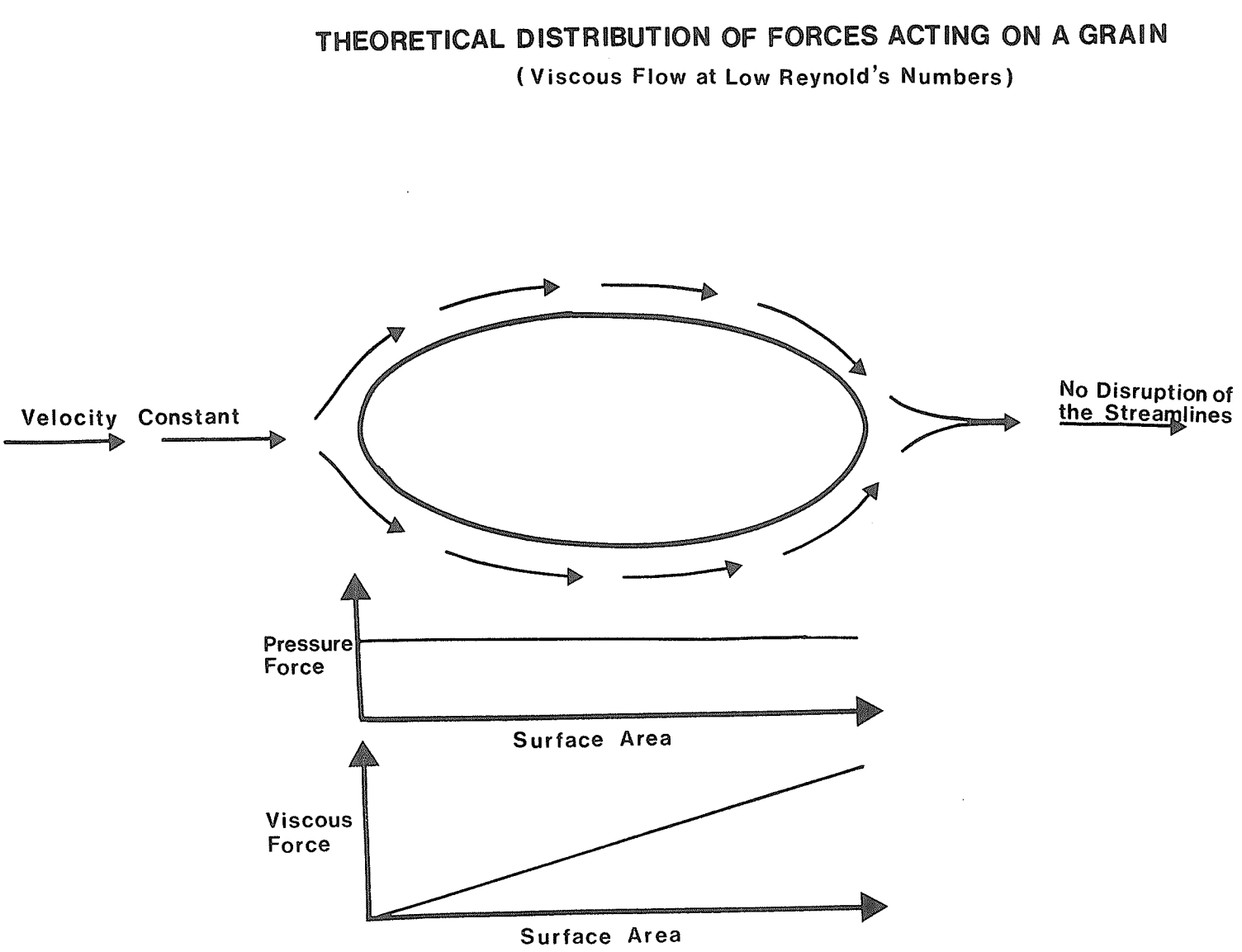
THEORETICAL DISTRIBUTION OF FORCES ACTING ON A GRAIN
(Viscous Flow at Low Reynold's Numbers)
Velocity Constant
No Disruption of the Streamlines
Pressure Force
Surface Area
Viscous Force
Surface Area

Figure 4.

front of the grain, increases to a maximum at the shoulder, and then decreases to a second stagnation point in the lee of the grain. The pressure distribution is the reverse of the velocity distribution, with maximum pressure being established at the nose of the grain, dropping to a minimum at the shoulder and then rising to a second maximum at the lee of the grain (Figure 5).

The boundary layer fluid particles are accelerated downstream due to the falling pressure gradient from the nose to the shoulder, achieving their maximum momentum at the shoulder. Since viscosity has opposed the movement of the fluid particles, their momentum at the shoulder is less than it otherwise might have been and their travel towards the tail not only starts with reduced momentum, but is also opposed by a rising pressure gradient. If this pressure gradient is too steep the boundary layer particles may slow to a stop or 'stall'. Once this occurs the adverse pressure field established by the main body of fluid will cause the boundary layer fluid to be pushed back behind the point of stall. This reversal in the direction of boundary layer flow utlimately produces a large eddying region of 'dead' flow and a disruption in the main flow, which must now pass around this dead region. The main body of fluid appears to separate from the grain surface which results in a reduction of pressure on the lee side and the development of form drag (Figure 6) (Shapiro, 1961, pp. 143-145).

It can be seen from this discussion that skin drag is the result of tangential fluid shear due to viscosity and occurs primarily under laminar flow conditions (low Reynold's numbers). The pressure imbalance that results from a stall of the boundary layer and subsequent separation of the main mass of fluid is known as 'form drag'. When this occurs the flow is said to be turbulent (very high Reynold's numbers).

Theoretical Pressure Distribution Over the Grain's Surface
(Viscous Flow at High Reynold's Numbers,
no Separation of the Boundary Layer)

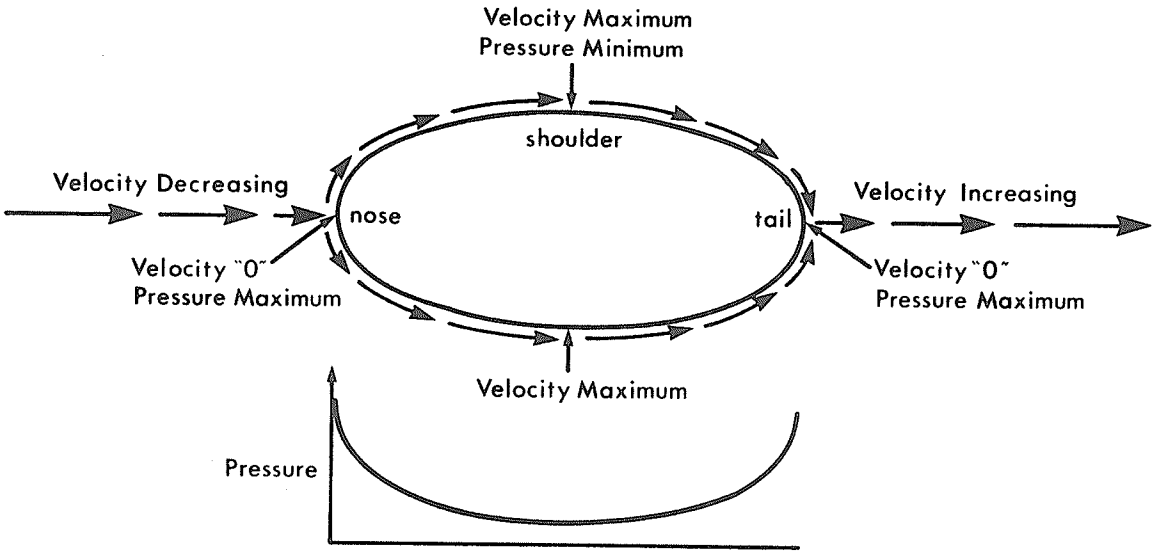

Figure 5.

Theoretical Pressure Distribution Over the Grain's Surface (Viscous Flow at Very High Reynold's Numbers, Stall and Separation of the Boundary Layer)

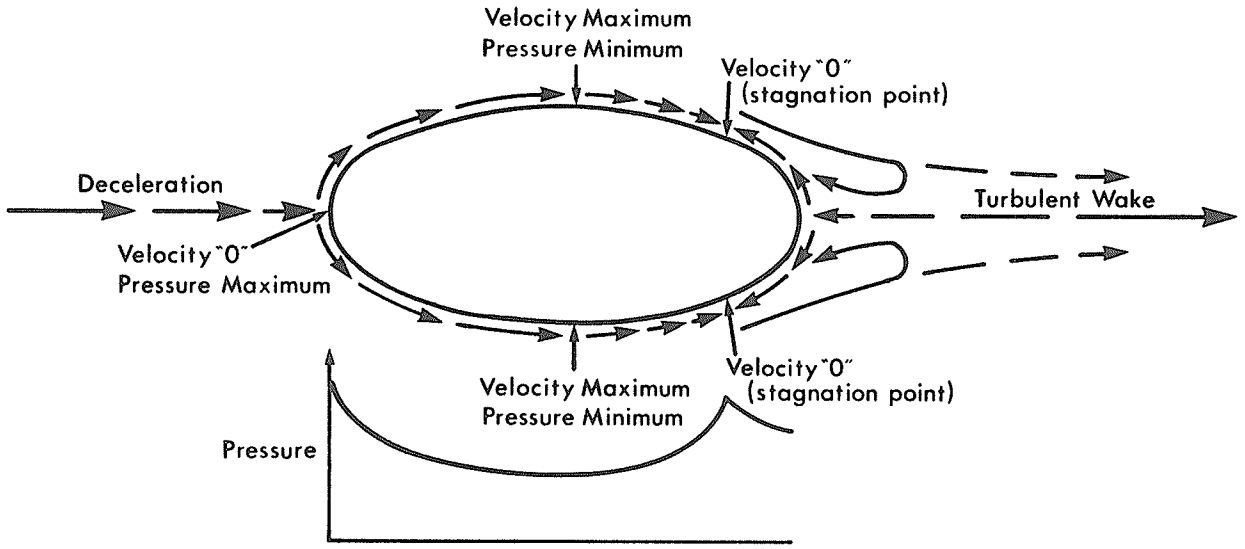

Figure 6.

2.4 Initiation of Particle Motion

Solid particles in an alluvial channel will begin to move when inertial grain resistance and the force of gravity holding the particle to the bed are exceeded by the fluid forces promoting movement. Coarse grains are also held in place by the frictional resistance provided by the surrounding particles, while fine grains may exhibit colloidal cohesion which binds groups of particles together.

White (1940) presented a simplified model which theoretically analyzed the fluid forces acting upon a spheroidal particle lying on a horizontal stream bed composed of similar sized grains. This model (Figure 7) equates the resistance to movement (the moment of weight, M_w) to the forces required for movement (the moment of drag, Md). He defined the critical shear stress required for movement as:

$$\tau_c = \eta \frac{\pi}{6} (\gamma_s - \gamma) D_s \tan \theta$$

where η is a dimensionless measure of the packing of the particles on the bed, $(\gamma_s - \gamma)$ is the submerged specific weight of the individual particles and D_s is the diameter of the spheroidal particle under examination. The formula be simplified by assuming a constant (k) for $\eta \frac{\pi}{6}$ (Leopold et al., 1964, p. 172) for which the value 0.18 may be substituted (Simons and Senturk, 1976, p.401).

The component forces acting to initiate movement under different flow regimes can be modelled in simple diagrams. When the flow is laminar, as indicated by a Reynold's number less than 500, viscous forces predominate and the flow contours the particle. The resultant drag force, skin drag, acts at a point above C in Figure 8. In this diagram θ is the submerged angle of respose, C is the centre of gravity and G is the point of support of the particle. The force due to gravity (Fg)

Moments on a Submerged Sand Particle Resting on a Horizontal Flat Bed at The Threshold of Movement

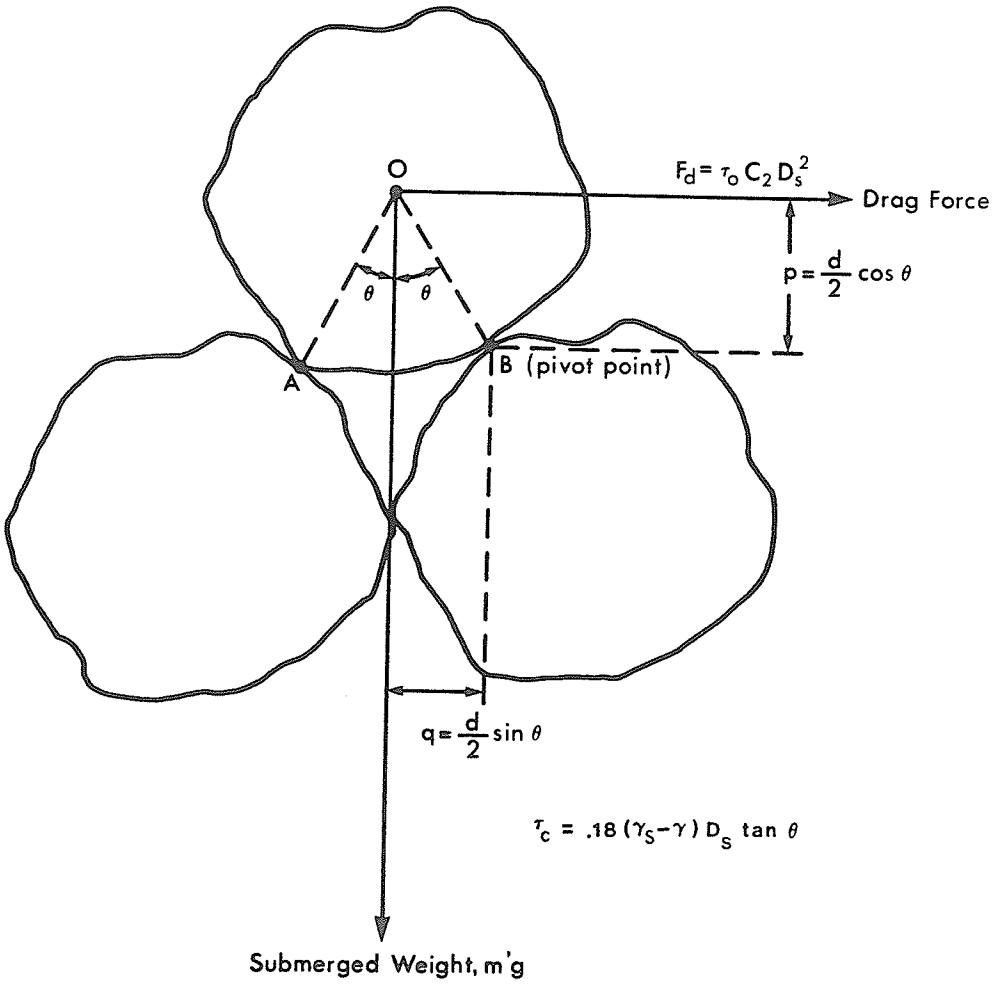

(White, 1940)

Figure 7.

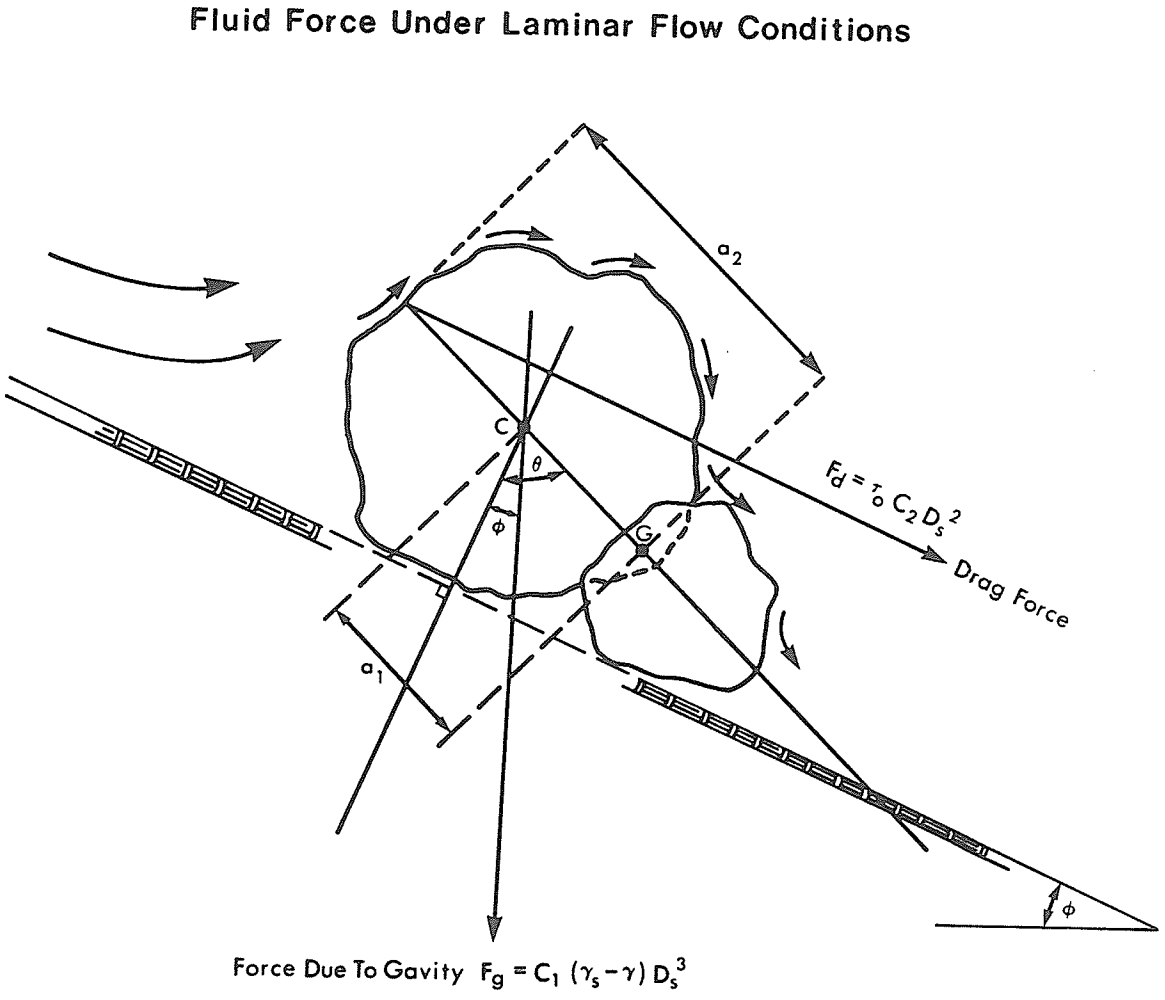

Simons and Senturk, 1976, p. 401

Figure 8.

which includes the buoyant force is given as:

$$Fg = C_1(\gamma_s - \gamma)\ D_s^3 \quad \text{(Simons and Senturk, 1976, p. 400)}$$

where C_1 is a form coefficient and D_s, γ_s and γ are as previously defined. The volume of the particle is $C_1 D_s^3$ and if the particle were spherical, $C_1 = \frac{\pi}{6}$. The drag force is expressed as:

$$Fd = \tau_o\ C_2 D_s^2, \quad \text{(Simons and Senturk, 1976, p. 402)}$$

where τ_o is the bed shear stress, $C_2 D_s^2$ is the effective surface area of the particle expressed to the shear stress and C_2 is a form coefficient defining the effective surface area. The simplified formula for the equilibrium of a particle on a sloping bed under laminar conditions thus becomes:

$$\tau_c = .18(\gamma_s - \gamma) D_s \tan\theta \quad \text{(Simons and Senturk, 1976, p. 401)}$$

Under turbulent flow conditions, inertial forces predominate and the resultant drag force operates at point C in Figure 9. The resultant drag force formula is the same as under laminar conditions, but an additional lift force component, F_L, resulting from turbulent velocity fluctuations and the Bernoulli effect is also operative. The total lift results from the vertical component of flow and the pressure distribution over the particles surface. This can be expressed as:

$$F_L = C_L C_3 D_s^2 \rho \frac{u^2}{2}, \quad \text{(Simons and Senturk, 1976, p. 404)}$$

where C_L is the coefficient of lift, C_3 is a form coefficient related to the effective surface area of the particle in the direction of lift, D_s^2 is the effective surface area of the particle, ρ is the density of water and u is the velocity of water near the particle. The resultant force (both lift and drag) is opposed by a gravitational force defined as:

$$F_g = C_1(\gamma_s - \gamma) D_s^3 \quad \text{(Simons and Senturk, 1976, p. 401)}$$

Fluid Force Under Turbulent Flow Conditions

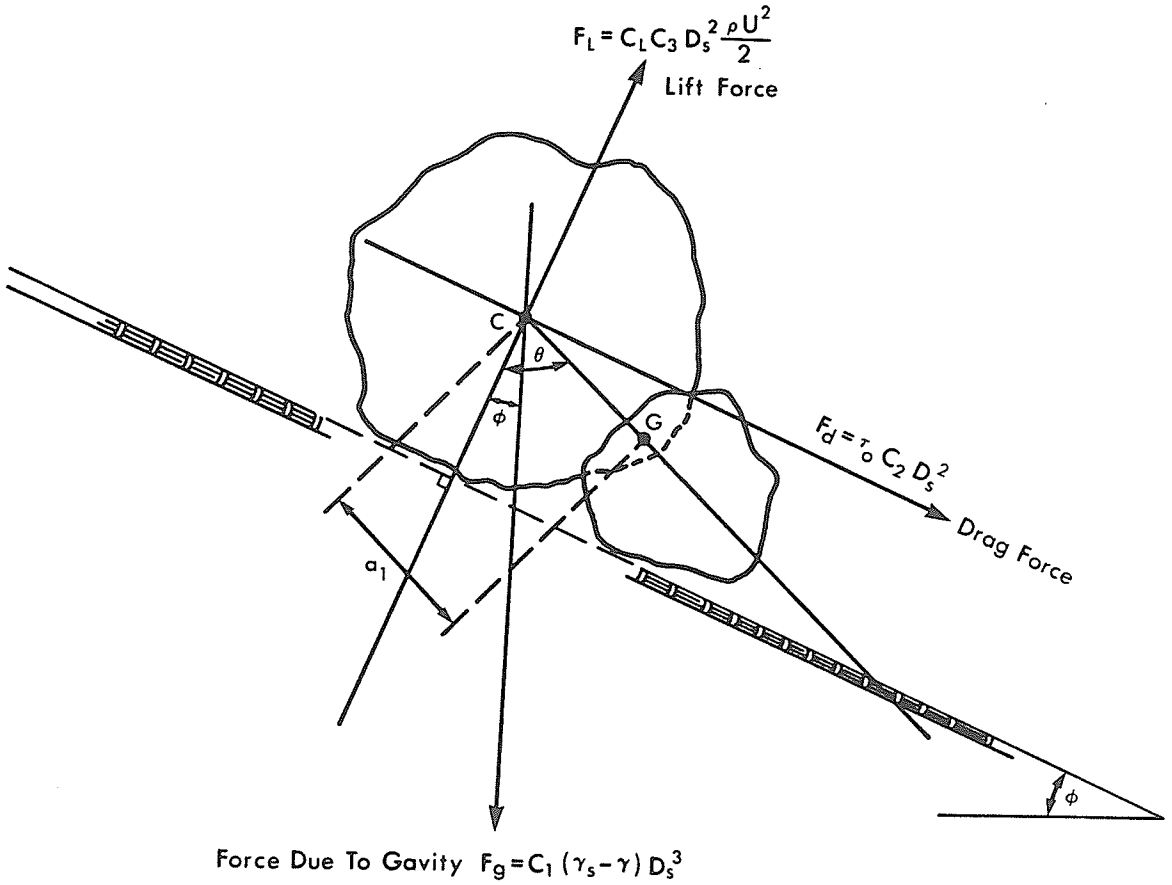

Simons and Senturk, 1976, p. 401

Figure 9.

where C_1 is a form coefficient and γ_s and D_s are as previously defined. In this model $a_1 = a_2$ where a_1 is the distance from the centre of gravity to the point of support and a_2 equals the distance from the point of support to the point of action of the resultant drag force. The equilibrium equation for a particle on a sloping bed under these conditions becomes:

$$\tau_c = k (\gamma_s - \gamma) D_s \tan \theta , \text{ with } k = \frac{C_1}{C_2}$$

(Simons and Senturk, 1976, p. 402)

2.5 Previous Research on Particle Entrainment

2.5.0 Introduction

The initiation of particle motion has been analyzed using two approaches. The theoretical approach utilized mainly by researchers in fluvial hydraulics, attempts to analyze and balance the dynamic and resistance forces to determine when resistance is overcome and particles will begin to move. The term critical tractive force is most often used as a measure of this threshold (Shields, 1936; White, 1940; Vanoni, et al., 1966). On the other hand, the majority of geomorphologists and engineers have employed empirical means to derive various critical erosion velocity measures (Hjulström, 1935, 1939; Rubey, 1938; Bagnold, 1954; Novak, 1973).

2.5.1 The Theoretical Approach

Numerous terms have been applied to describe the motivating force at work to overcome a particle's resistance to movement. DuBoys in 1879 called it tractive force; White (1940) described it as shear stress; Flaxman (1966) used the term tractive power; and Yang (1973) explained the ability of water to move particles as unit stream power. These researchers all realize that flow characteristics within the boundary

layer are difficult, if not impossible, to measure and they attempt to relate measurable parameters to the boundary layer condition. The complexity and variability of both the resisting and motivating forces cause even the most complex formula to be an over simplification of the real condition.

The theoretical approach, employing the critical shear stress concept, is best exemplified by White's (1940) research which has been previously discussed. His original formula can be criticized on the grounds that he ignored the influence of lift forces on the equilibrium condition. Shields (1936) presented a graphical solution to this concept of particle motion showing it to be the result of tangential fluid shear. This is the widely accepted Shields' diagram (Figure 10), where the tractive force coefficient $F_* = \frac{\tau_c}{\gamma_s - \gamma}$ is plotted against the boundary Reynold's number $R_* = \frac{U_* D_s}{\nu}$, where U_* is shear velocity and ν is the kinematic viscosity.

There has been some criticism of Shield's diagram. Yang (1973) reasons that it is inappropriate to plot shear stress against shear velocity since they are interrelated to $U_* = \sqrt{\frac{\tau}{\rho}}$. Baker and Ritters' (1975) analysis dealing with observations of incipient motion in natural streams showed results which were at variance with those predicted by the Shields' diagram. The diagram is based only on tangential forces even though lift forces do occur within natural streams. Baker and Ritter felt that lift will be maximized in very shallow streams where velocity gradients are steepest and that the competence of these streams is underestimated by the Shields' diagram (Baker and Ritter, 1975, p. 976).

The magnitude of the lift force has been the subject of some debate. Simons and Senturk (1976) cite Askoy's (1973) experiments, where the lift force fluctuated around 1/7th of the drag force, and Coleman's

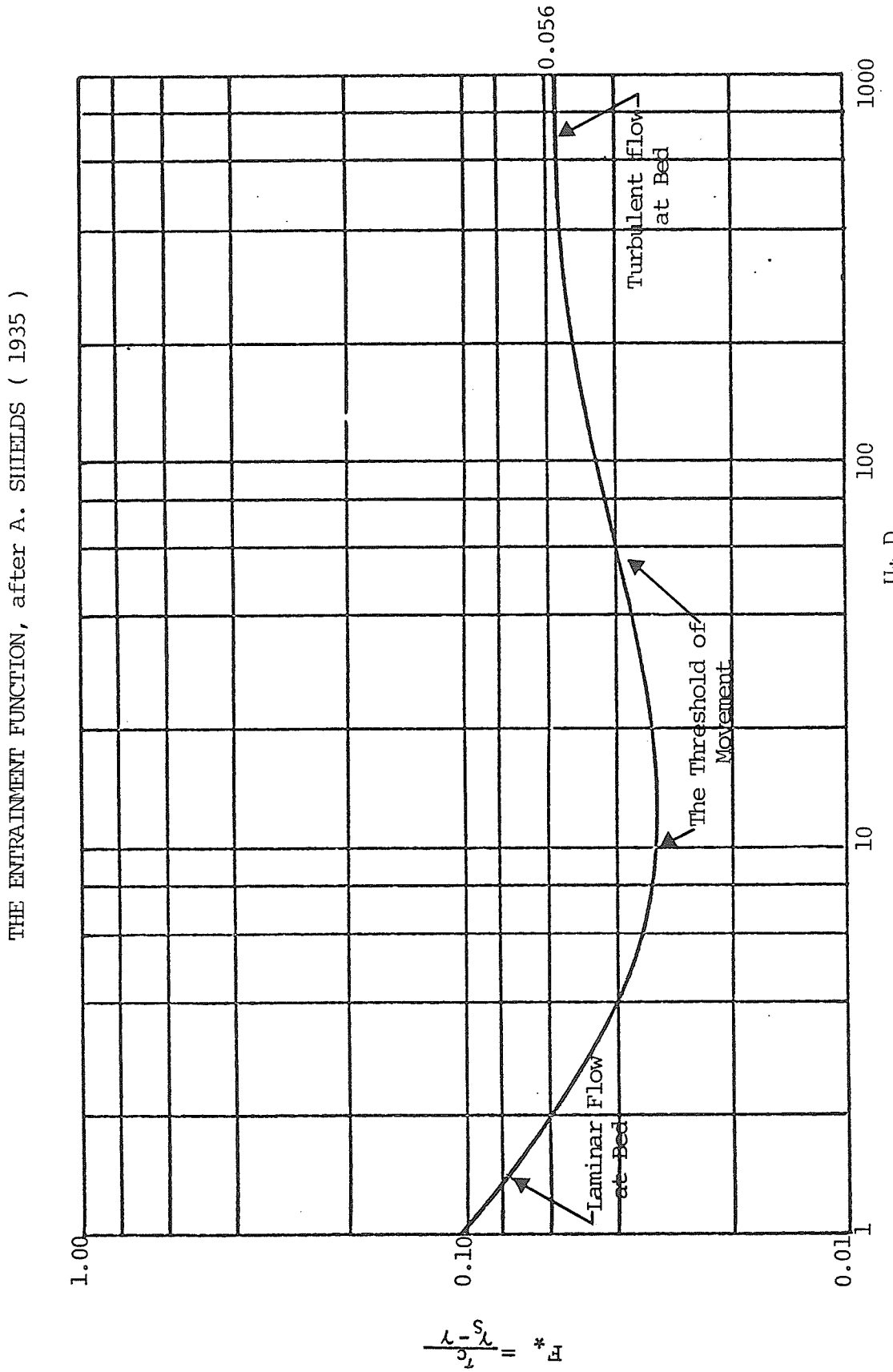
THE ENTRAINMENT FUNCTION, after A. SHIELDS (1935)
1.00
0.10
0.01
0.056
1
10
100
1000
Turbulent Flow at Bed
The Threshold of Movement
Laminar Flow at Bed
$F_* = \frac{\tau_c}{\gamma_s - \gamma}$
$R_* = \frac{U_* D_s}{\nu}$

Figure 10.

(1972) experiments, where the ratio was about unity. Chepil's (1961) study similarly showed that the lift force close to the boundary was comparable in magnitude to the drag force for particles on the bed. The lift force decreases rapidly as the particles move away from the bed as a result of the rapid decrease in the velocity gradient.

While White's and similar tractive force formulae (Shields, 1936; Gessler, 1971) are supported by numerous laboratory experiments, application to stream channels has not been that successful (Lane and Carlson, 1953; Baker and Ritter, 1975).

2.5.2 The Empirical Approach

The empirical approach to the initiation of particle motion is typified by the work done by Hjulström (1935, 1939). He utilized an erosion velocity as a measure of the motivating force. His erosion velocity was the average cross-sectional velocity in a flume with a water depth of one meter. From this he constructed a diagram relating the critical velocity needed to initiate movement to the diameter of the uniform sized particles. These conditions of uniform water depth and particle size are uncharacteristic of natural rivers, where uniform flow depth seldom occurs and where bed material is of variable size. Practical application of the Hjulström diagram (Figure 11) is thus limited.

Flume studies, similar to Hjulström's, have been used by many researchers to derive formulae relating particle size and critical velocity. Most researchers investigating erosion velocities for gravel sized particles, have found their experimental results to be best represented by a power function of the form: $V_* = C\ D_s^n$, where V_* is critical velocity, C is a constant, D_s is the particle diameter and 'n' an empirical exponent (e.g. Bogardi and Yen, 1938, Tu and Ho, 1938;

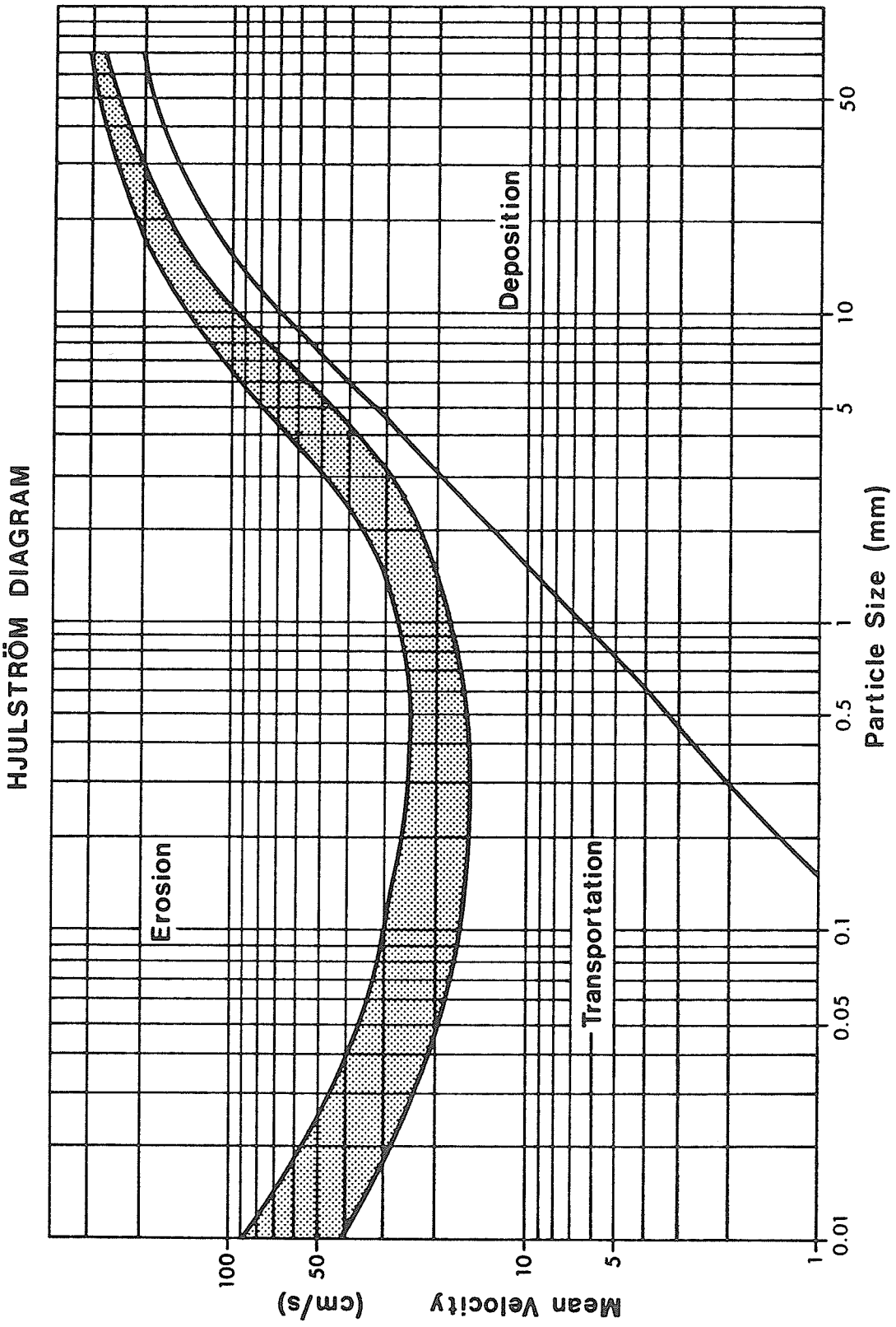
HJULSTRÖM DIAGRAM
Erosion
Deposition
Transportation
Mean Velocity (cm/s)
100
50
10
5
1
Particle Size (mm)
0.01
0.05
0.1
0.5
1
5
10
50

Figure 11.

Velikanov, 1948; Kalmar, 1952; Bagnold, 1954; Neill, 1967; Bogardi, 1974). Those formulae, which employ the mean cross-sectional velocity (V_{mc}) as the operational definition of the critical erosion velocity, show little variability in the exponent 'n'.

The results of empirical studies involving natural channels (Galay, 1971; Novak, 1973) deviate from those predicted by controlled flume modelling (e.g. Hjulström, 1935). Novak (1973) suggests that these discrepancies may be due to several factors:

i) various operational definitions of erosion velocity terms, e.g. the bottom erosion velocity (Bogardi and Yen, 1938) and the mean cross-sectional velocity (Hjulström, 1935);

ii) the effect of flow depth on velocity gradients and associated shear stresses;

iii) the effect of suspended sediment load, channel pavements and various bed forms;

iv) the use of uniform size, spheroidal bed material in flume studies.

In addition, Novak (1973) proposes that the difference between naturally observed erosion velocities and comparable critical erosion velocities measured in flumes is even more significant when gravel size material is being considered.

Keller (1970) conducted bed-load movement experiments along a pool and riffle reach of an intermittent stream in California. He derived an effective bed velocity formula:

$$\text{EBV (effective bed velocity)} = \frac{MX_s + N_p\ 6.32 + N_r\ 3.69}{N_p + N_r + 1}$$

where MX_s equals the maximum starting velocity, N_p is the number of pools and N_r is the number of riffles. This was an attempt to take bed

morphology into consideration, although the lack of direct measurements of bed velocity at the time of incipient particle motion makes the application questionable.

Helley (1969) studied the movement of coarse bed materials in a California river. In this study he attempted to measure bed velocity, which he considered the dominant parameter affecting particle motion. Bed velocity was measured at 0.6 of the height of the particle from the bed, this being the centroid of the drag force in his evaluation. The measured results he obtained coincided closely with those predicted by his bed velocity formula. Of the factors he considered in the initiation of particle motion shape and size appear to predominate, while specific gravity and orientation angle have much less influence.

Bottom or bed velocity has been recognized by many researchers to be theoretically a more appropriate measure of critical erosion velocity than mean cross-sectional velocity (Rubey, 1937; Bogardi, 1974). Direct measurement of bottom velocity is, however, impossible and more or less arbitrary assumptions concerning the velocity profile and the depth to which it extends into the bed have been employed to define this measure (c.f. Bogardi, 1974, p. 90). Because of the difficulties associated with these assumptions studies employing bottom velocity are relatively rare and the comparability of results limited. Although the relationship between mean cross-sectional velocity and bottom velocity has not been definitely established, a general relationship between the two velocity terms may be assumed. Bogardi and Yen (1938) demonstrated that under comparable conditions the erosion velocity associated with bottom velocity, was of a lower magnitude than the erosion velocity associated with mean cross-section velocity measures. In more recent studies Bogardi substantiates these results (Bogardi, 1974).

2.6 Justification for Further Research

Experimental research into incipient particle motion has, for the most part, evaluated the critical condition for uniform size, non-cohesive, spherical grains lying on a horizontal or gently sloping bed. These conditions do not exist in natural streams and the assumption of such conditions reduces the accuracy with which incipient motion can be predicted for natural streams.

Galay (1971 and 1972) compared the experimental results of several researchers employing flume studies (Izbash, 1936; Hallmark and Smith, 1965; and Bhowmik and Simons, 1970) with the formula he developed for natural streams. The empirical relationship demonstrated by the flume studies all fell into the general form, $V_{mc} = aD^{\frac{1}{2}}$, where a is an empirical constant and D represents the median size of well sorted, spherical particles. Galay's study of the movement of large rocks in Canadian and American rivers indicates that the slope of the plotted line may be somewhat flatter. This might be attributed to the non-spherical shapes, non-uniform grain sizes and the variety of bed forms found in streams.

Flume modelling, however, still serves two very important functions. It allows for the development of erosion velocity formulae for atypical sediment when time restraints make field observations infeasible. Flume modelling can also be used to empirically evaluate the effect of sediment parameters on the initiation of particle motion when it is not possible to do so theoretically. The relationships between sediment characteristics (other than size) and incipient motion are poorly understood and thus are worthy of further investigation.

Bogardi (1974) reviews several flume experiments (Bogardi and Yen, 1938; Velikanov, 1948; Kalmar, 1952; and Neill, 1967) which investigate

the relationship between various erosion velocities (V_*) and particle size (D_s). He indicates that there is considerable variation in the constants and exponents of the various power functions, and that large deviations from the mean values (constant = 26.7 ± 0.12) reflect different particle specific gravities, variations in the operational definition of erosion velocity and different flow depths within the flumes.

Galay (1971), Novak (1973), and Bogardi (1974), indicate that further studies of erosion velocity for natural riverine gravels are required. Further flume experiments are also required to investigate the effect of shape, specific gravity and flow depth on incipient particle motion.

CHAPTER 3

METHODOLOGIES

3.1 Introduction

To this point it has been stressed that the study of incipient particle motion is complex. Although the two main schools of thought have offered much to further our understanding of the processes involved, it can be argued that by their very nature, empirical studies are more easily adapted to a real world situation.

The frequency of sediment transport can be estimated by knowing the empirical relationship between particle size and critical erosion velocity, and determining the frequency with which velocities sufficient to cause movement are achieved. Empirical studies, however, have tended to evaluate incipient motion for sediment composed of spheroids having a specified gravity of 2.65. It is necessary, therefore, when attempting to relate sediment transport and stream velocities in the Riding Mountain area, that an empirical study of incipient motion for the shale gravels found in these watersheds be conducted. Even this, however, only establishes the theoretical relationship between shale particle movement and water velocity. To make practical application of this knowledge requires a data base encompassing sediment characteristics, channel morphology and the frequency and magnitude of stream flows.

This chapter presents the methodologies employed in:

a) the selection of sampling sites;

b) the determination of bed load characteristics;

c) the examination of the weathering process;

d) the determination of a regional flood frequency;

e) the establishment of the relationship between shale particle size and critical erosion velocity;

f) the synthesis of these studies to determine the frequency of sediment movement for selected locations in the three study streams.

3.2 Selection of Sampling Sites

Although the Riding Mountain watersheds can be viewed as being topographically and hydroclimatically similar, stream channel morphology and specific sediment characteristics must be examined before the frequency of fluvial transport for the area can be ascertained. Sample sites were thus selected for two purposes; to present the specific characteristics of the stream channel and to demonstrate the similarities which exist between sites on different streams within the study area.

The suitability of a stream site was based upon the following:

1) spatial and temporal accessibility;
2) the absence of vegetation;
3) the absence of noticeable interference of the bed material by animal or man.

The examined streams had to have at least three acceptable sampling locations along their length. Potential sites were first identified from air photographs and topographic maps. Field reconnaissance eliminated all but 17 sites; seven along Eden Creek, five along Birnie Creek and five along Wilson Creek. Morphometric measurement and bedload sampling was conducted at all sites. In addition, the sites along Eden Creek were chosen to investigate weathering under natural conditions.

The locations selected are indicated in Figure 3.

3.3 Determination of Sediment Characteristics

3.3.1 Bedload Sampling

Examination of bedload sediment was conducted to determine the size distributions and shape characteristics at the selected sites. Spatial and temporal variations were then noted so that the pattern of size and shape characteristics along each stream and for the area as a whole could be established.

Systematic random sampling of fifty rocks per site was carried out three times during the five-month summer field season. Rocks were selected using a one meter square sampling grid divided at 10 centimeter intervals by monofilament line. The junctures between these lines became sampling points and one-half of these points provided the sample number.

The lengths of the three principal axes (long (a), intermediate (b), and short (c)) of each rock sampled were measured. Particle size was defined by calculating the diameter (d) of a sphere with an equivalent volume, using the formula, $d = \sqrt[3]{a\ b\ c}$ (Folk, 1965, p. 8). This is called the nominal diameter of the rock and gives a better indication of the volumetric size of the particles than any of the individual axial measurements. The use of nominal diameter produced grain size distributions which more accurately represent the size distributions than the b-axis value normally used for this purpose. Comparison of grain size distributions and application of the critical erosion velocity formula could thus be carried out with a greater degree of confidence.

The Corey (1949) Shape Factor and the Zingg (1935) diagram were

used in evaluating particle shape. The Corey Shape Factor ($Sp = \frac{c}{\sqrt{a.b}}$) is a numerical value indicating how closely the particle resembles a sphere, with the value for a perfect sphere being 1.0. The Zingg diagram qualitatively describes particle shape using the ratios between the principal axes $^{b}/_{a}$ and $^{c}/_{b}$.

A Watfiv program (Appendix 1) computed the nominal diameter, the Corey Shape Factor, $^{b}/_{a}$ and $^{c}/_{b}$ ratios, and ranked the size values. The Cailleux (1945) flatness index $i = \frac{a + b}{2c}$ was used to characterize the flatness of the shale particles.

The mean and standard deviations of size and shape characteristics for each sample are presented in Table 1. Comparisons of the means of the samples were performed using a t-test to determine whether there were any significant differences in grain size between samples collected during the same period along each stream and whether any changes in grain size occurred over the season.

On Birnie Creek only 50% of the comparisons revealed a statistically significant difference between samples collected at adjacent sites, whereas this rose to 63% when comparisons were made between all samples collected during the same period. No significant change in grain size between one sampling period and the next was shown by 60% of the tests, although this was reduced to 40% in comparisons made between samples collected in the first and last sampling periods.

Comparisons performed on samples collected along Wilson Creek produced similar results. T-tests comparing samples from adjacent sites showed a statistical difference in grain size in 50% of the cases. This value increased to 60% when comparisons were made between all samples collected on Wilson Creek during the same sampling period. A significant change in grain size was shown by all comparisons performed

TABLE 1

MEANS AND STANDARD DEVIATIONS OF

BEDLOAD SAMPLE CHARACTERISTICS

Eden Creek

Nominal Diameter (cm)

	Sample Period 1		Sample Period 2		Sample Period 3	
	Mean	Standard Deviation	Mean	Standard Deviation	Mean	Standard Deviation
Site Number 1	1.97	0.78	1.90	1.00	2.26	0.69
2	1.65	0.59	1.49	0.67	2.01	0.72
3	1.18	0.40	1.05	0.30	1.33	0.34
4	2.36	0.84	1.92	0.58	1.70	0.48
5	1.29	0.49	1.78	0.88	1.87	0.62
6	1.89	0.69	1.80	0.65	1.94	0.57
7	1.94	0.64	1.91	0.63	1.93	0.59

Corey Shape Factor

	Sample Period 1		Sample Period 2		Sample Period 3	
	Mean	Standard Deviation	Mean	Standard Deviation	Mean	Standard Deviation
Site Number 1	0.19	0.10	0.20	0.08	0.23	0.08
2	0.18	0.09	0.17	0.07	0.20	0.08
3	0.20	0.09	0.20	0.06	0.20	0.06
4	0.22	0.09	0.19	0.06	0.22	0.09
5	0.22	0.15	0.19	0.07	0.20	0.08
6	0.22	0.10	0.20	0.08	0.24	0.09
7	0.22	0.10	0.20	0.08	0.24	0.09

$^{b}/_{a}$ Ratio

	Sample Period 1		Sample Period 2		Sample Period 3	
	Mean	Standard Deviation	Mean	Standard Deviation	Mean	Standard Deviation
Site Number 1	0.65	0.19	0.67	0.15	0.67	0.17
2	0.65	0.14	0.66	0.13	0.58	0.17
3	0.66	0.16	0.69	0.15	0.71	0.16
4	0.64	0.15	0.72	0.14	0.69	0.15
5	0.71	0.13	0.69	0.12	0.74	0.17
6	0.64	0.18	0.71	0.15	0.71	0.17
7	0.67	0.18	0.70	0.17	0.68	0.15

$^{c}/_{b}$ Ratio

	Sample Period 1		Sample Period 2		Sample Period 3	
	Mean	Standard Deviation	Mean	Standard Deviation	Mean	Standard Deviation
Site Number 1	0.25	0.12	0.26	0.11	0.29	0.10
2	0.23	0.11	0.21	0.09	0.27	0.11
3	0.27	0.14	0.25	0.09	0.24	0.09
4	0.28	0.12	0.23	0.07	0.27	0.13
5	0.26	0.18	0.23	0.10	0.24	0.11
6	0.28	0.12	0.25	0.10	0.24	0.17
7	0.27	0.13	0.25	0.15	0.30	0.11

Birnie Creek

Nominal Diameter (cm)

	Sample Period 1		Sample Period 2		Sample Period 3	
	Mean	Standard Deviation	Mean	Standard Deviation	Mean	Standard Deviation
Site Number 1	3.21	1.34	2.51	1.07	2.73	1.22
2	3.27	1.37	3.08	1.56	2.72	0.90
3	2.30	1.22	2.14	0.89	2.64	0.81
4	2.03	0.62	1.72	0.66	2.62	0.77
5	1.71	0.64	1.99	0.93	2.29	0.58

Corey Shape Factor

	Sample Period 1		Sample Period 2		Sample Period 3	
	Mean	Standard Deviation	Mean	Standard Deviation	Mean	Standard Deviation
Site Number 1	0.19	0.07	0.19	0.06	0.18	0.06
2	0.21	0.09	0.19	0.08	0.20	0.08
3	0.23	0.10	0.19	0.07	0.21	0.06
4	0.21	0.08	0.17	0.08	0.19	0.07
5	0.21	0.06	0.18	0.07	0.21	0.07

$^{b}/_{a}$ Ratio

	Sample Period 1		Sample Period 2		Sample Period 3	
	Mean	Standard Deviation	Mean	Standard Deviation	Mean	Standard Deviation
Site Number 1	0.64	0.18	0.68	0.16	0.67	0.17
2	0.71	0.16	0.69	0.17	0.68	0.17
3	0.67	0.15	0.67	0.19	0.71	0.14
4	0.67	0.16	0.65	0.17	0.72	0.18
5	0.69	0.16	0.65	0.18	0.69	0.16

$^{c}/_{b}$ Ratio

	Sample Period 1		Sample Period 2		Sample Period 3	
	Mean	Standard Deviation	Mean	Standard Deviation	Mean	Standard Deviation
Site Number 1	0.28	0.16	0.24	0.09	0.23	0.08
2	0.27	0.16	0.24	0.10	0.26	0.11
3	0.29	0.14	0.24	0.10	0.25	0.09
4	0.27	0.12	0.22	0.11	0.24	0.12
5	0.26	0.09	0.24	0.11	0.26	0.10

Wilson Creek

Nominal Diameter (cm)

	Sample Period 1		Sample Period 2		Sample Period 3	
	Mean	Standard Deviation	Mean	Standard Deviation	Mean	Standard Deviation
Site Number 1	2.96	1.07	2.06	1.25	2.95	0.81
2	2.34	1.03	1.79	1.05	3.07	0.92
3	1.92	0.94	1.54	0.82	1.84	0.62
4	2.17	0.83	1.66	0.92	2.32	0.82
5	1.84	0.99	1.27	0.93	1.64	0.60

Corey Shape Factor

	Sample Period 1		Sample Period 2		Sample Period 3	
	Mean	Standard Deviation	Mean	Standard Deviation	Mean	Standard Deviation
Site Number 1	0.22	0.10	0.21	0.11	0.22	0.10
2	0.21	0.07	0.23	0.14	0.23	0.09
3	0.20	0.08	0.19	0.10	0.19	0.07
4	0.21	0.08	0.19	0.21	0.21	0.08
5	0.22	0.10	0.17	0.11	0.20	0.09

$^{b}/_{a}$ Ratio

	Sample Period 1		Sample Period 2		Sample Period 3	
	Mean	Standard Deviation	Mean	Standard Deviation	Mean	Standard Deviation
Site Number 1	0.70	0.16	0.68	0.17	0.66	0.16
2	0.70	0.18	0.68	0.17	0.67	0.14
3	0.72	0.15	0.69	0.17	0.65	0.17
4	0.67	0.19	0.67	0.17	0.69	0.15
5	0.66	0.17	0.68	0.14	0.63	0.17

$^{c}/_{b}$ Ratio

	Sample Period 1		Sample Period 2		Sample Period 3	
	Mean	Standard Deviation	Mean	Standard Deviation	Mean	Standard Deviation
Site Number 1	0.29	0.15	0.27	0.15	0.28	0.15
2	0.26	0.11	0.30	0.19	0.29	0.12
3	0.24	0.10	0.25	0.14	0.24	0.11
4	0.27	0.11	0.27	0.16	0.25	0.10
5	0.28	0.13	0.24	0.18	0.26	0.14

on samples collected from the same site during different sampling periods.

The mean grain size of samples collected from adjacent sites on Eden Creek were found to be significantly different in 56% of the cases. This value increased to 63% when all samples collected along this stream during the same sampling period were compared. Significant grain size change was not shown in 57% of the comparisons performed between samples collected during different periods.

All samples collected have a similar mean Corey Shape Factor despite the large standard deviations found. The average Corey shape is .20 indicating that the particles bear little resemblance to the spheroids used in most theoretical analyses and empirical experiments.

The average shale particle may also be described as oblate in terms of Zingg's (1935) descriptive classification. This particle would have $^{b}/_{a}$ and $^{c}/_{b}$ ratios of .677 and .257, respectively. The $^{b}/_{a}$ value is close to the boundary value of .667 which indicates that the average shale particle is close to blade-like in shape and in 35% of the samples the blade shape predominates. A Cailleux (1945) flatness index of 4.79 characterizes the average flatness of the shale particles.

3.3.2 Weathering of Shale Sediments

The majority of the bedload sediment is provided by weathering of shale bedrock. It was believed that hydration weathering was responsible for the reduction in particle size both on exposed bedrock outcrops and on point bars. To ascertain whether there was a significant decrease in grain size over the field season seven sites along Eden Creek were sampled and photographed at two week intervals over a three month period. Eden Creek's accessibility and variable flows made it most suitable for an investigation of weathering under natural conditions.

Periodic high flows inundate the gravel bars along the stream and facilitate the hydration weathering process.

Weathering sites were permanently established by means of a stake on exposed bars adjacent to bedload sampling sites. The stake served as a guide to positioning a $0.25m^2$ sampling grid for photographic purposes, and also served as a starting point for line transects used in collecting 50 rock samples.

Photographing a specified section of an exposed bar was undertaken to allow measurement of size changes for individual shale particles through the field season. In this way, weathering could be observed in the natural environment without disturbing the arrangement of particles.

The size of each rock collected was determined by calculating its nominal diameter, and size distributions for each sample were constructed. Comparisons between samples from the same location were undertaken to evaluate progressive changes.

A t-test was employed to test the hypothesis that there was a significant decrease in particle size from one period to the next at each sample site. The same procedure was also employed to ascertain whether size had decreased over the course of the field season. The results of this study were inconclusive, with only 32.4% of the 105 comparisons showing significant decreases in size. It is believed that these results can be attributed to several factors. The weathering process requires that the shale particles be subjected to extremes in moisture, whereby variable rates of expansion due to absorption of water into a dry rock causes it to fracture. Preliminary reports by the Manitoba Water Resources Branch and field observation indicate that these extremes did not occur during the 1978 field season. Stream flows during the summer were fairly constant and because of this rocks

on dry bars remained dry. As well, rocks nearer the stream on bars which were moist at the beginning of the season remained moist due to absorption through their basal surfaces. The encroachment of vegetation also provided a degree of protection ensuring that the rapid moisture changes condusive to the weathering process did not occur.

The lack of significant results on weathering from field observations necessitated a controlled laboratory study of the weathering process. A large bedload cobble (Plate 1), initially immersed in water, was subjected to a sequence of three drying and two wetting periods. After each phase the rock and its fragments were photographed and measured to document the decrease in particle size and to determine whether hydration or dehydration was the dominant weathering process.

The wetting cycle involved immersion in water for a one hour period. The particle was then air dried until no further breakage or sign of surface moisture was exhibited. The results of this study are presented in Table 2. Nominal diameter is again employed as it gives an indication of the volumetric size changes.

During the initial drying period cracks appeared in the surface of the cobble although it remained intact (Plate 2). Re-wetting caused the rock to fracture into sixty-five separate angular pieces (Plate 3). Drying resulted in further breakage of four of the fragments. One fragment broke into six pieces, two into three pieces and one into two pieces (Plate 4). In step five, the last wetting sequence, four fragments broke into two pieces and one into five (Plate 5). The smaller pieces numbered from 30 to 61 did not break. During the final drying phase two fragments broke into four and two pieces, respectively (Plate 6). It can be seen from Table 2 that

LABORATORY WEATHERING EXPERIMENT STAGE 1

Plate 1

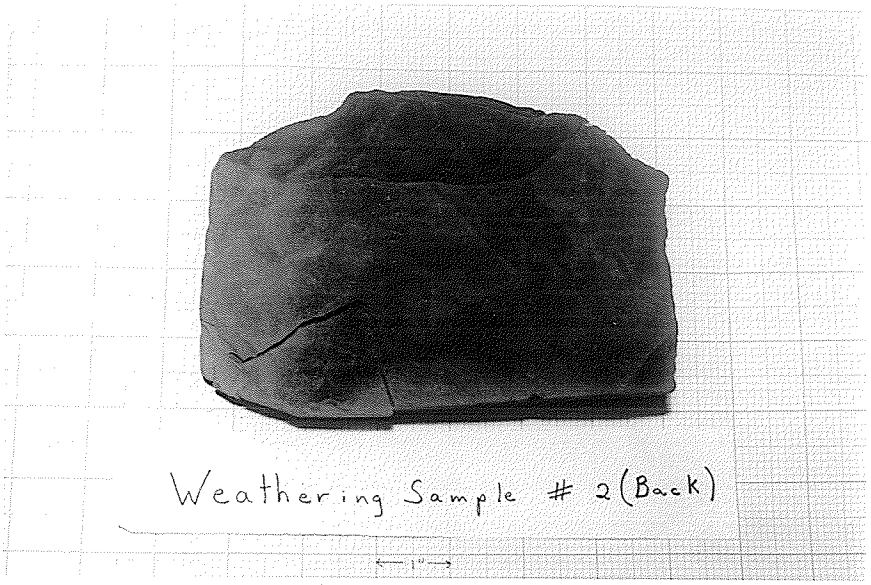

LABORATORY WEATHERING EXPERIMENTS STAGE 2

Plate 2

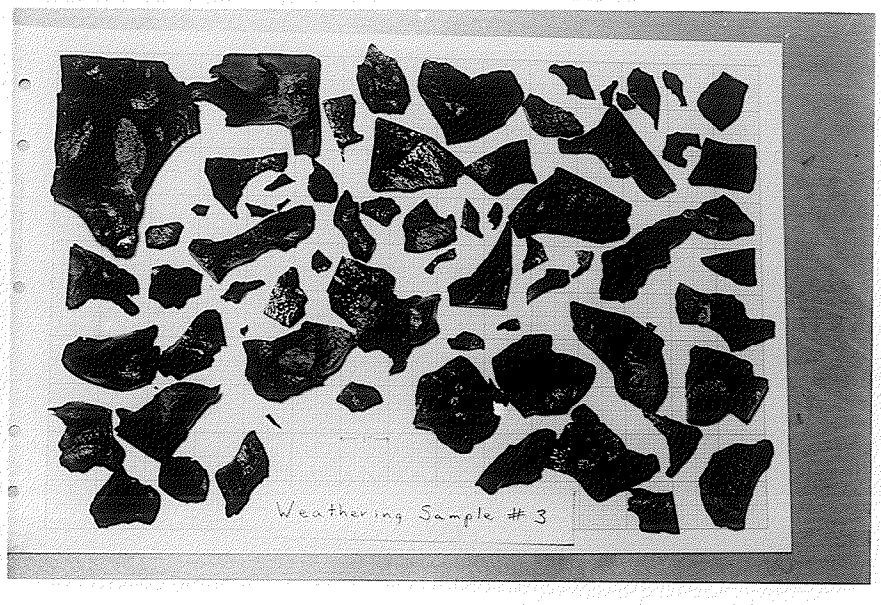

LABORATORY WEATHERING EXPERIMENTS STAGE 3

Plate 3

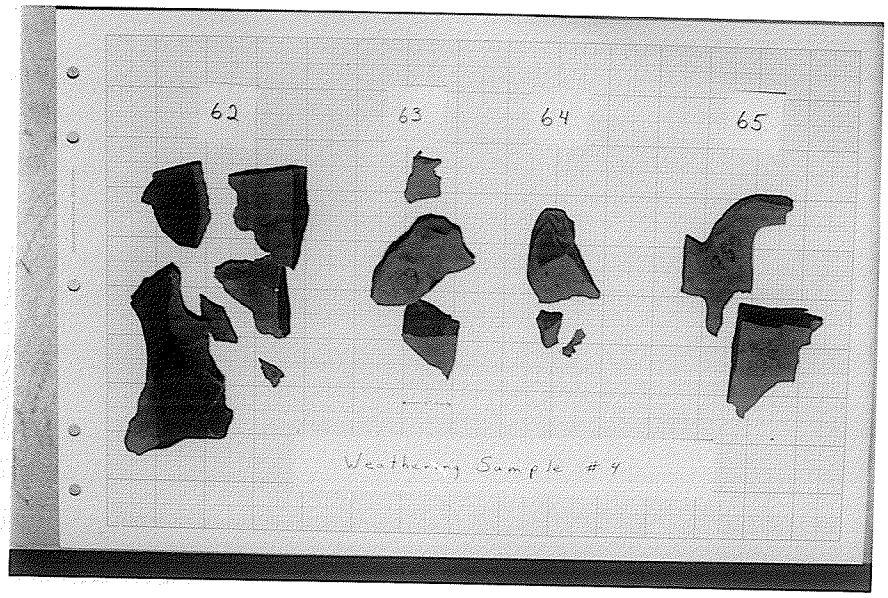

LABORATORY WEATHERING EXPERIMENTS STAGE 4

Plate 4

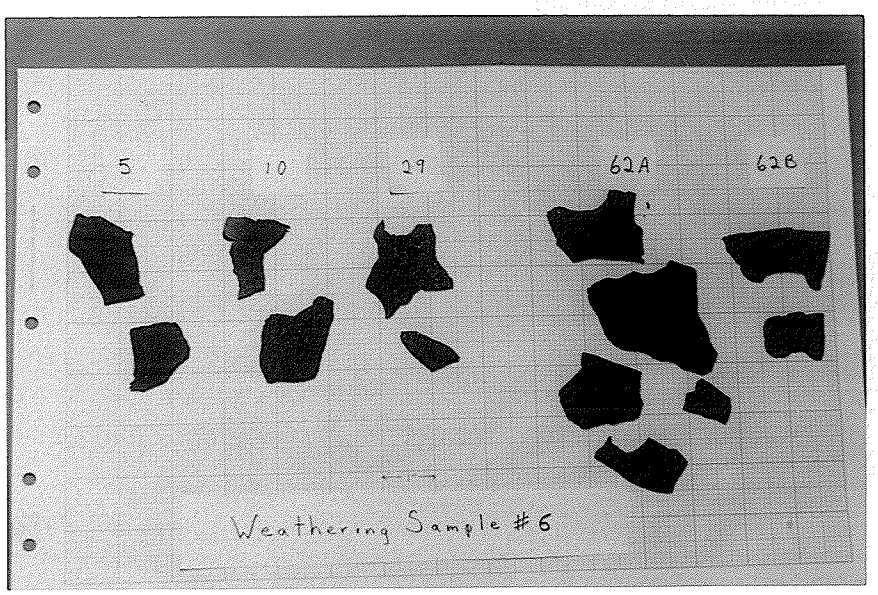

LABORATORY WEATHERING EXPERIMENTS STAGE 5

Plate 5

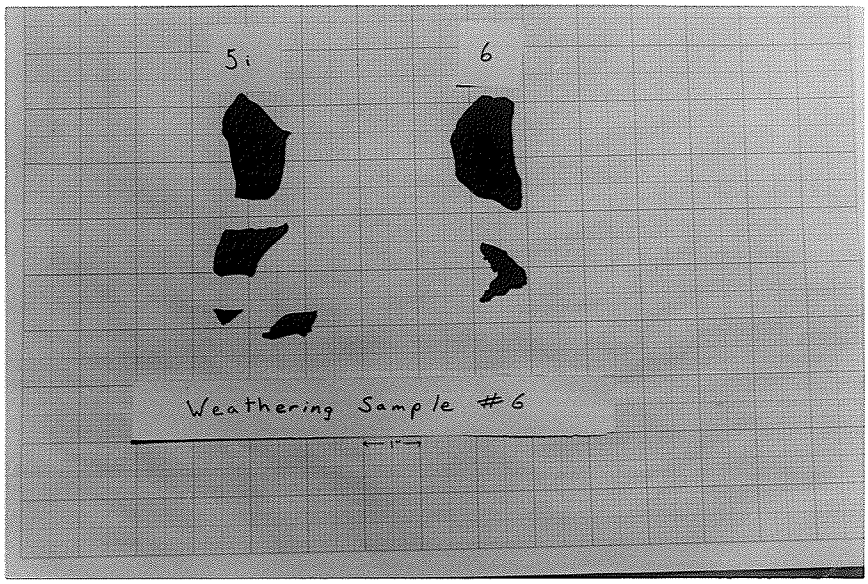

LABORATORY WEATHERING EXPERIMENTS STAGE 6

Plate 6

TABLE 2

RESULTS OF LABORATORY WEATHERING

Stage 1	Stage 2	Stage 3	Stage 4	Stage 5	Stage 6
					5ia)2.46(.34)
		1)3.08(0.26)			5ib)1.46(.14)
		2)3.42(0.37)			5ic)1.02(.29)
		3)2.76(0.19)			5id)0.65(.32)
		4)2.90(0.25)		5i)2.66(0.38)	
		5)3.11(10.33)		5ii)2.14(0.42)	
		6)2.83(0.46)			6a)2.79(0.53)
		7)2.87(0.34)			6b)1.02(0.16)
		8)3.26(0.48)			
		9)2.28(0.25)			
		10)2.68(0.25)		10i)2.00(0.21)	
		11)3.16(0.47)		10ii)2.52(0.27)	
		12)2.62(0.24)			
		13)2.31(0.29)			
		14)2.04(0.27)			
		15)2.10(0.12)			
		16)2.38(0.29)			
		17)2.10(0.24)			
		18)2.08(0.29)			
		19)1.84(0.23)			
		20)1.81(0.21)			
		21)2.51(0.46)			
		22)2.13(0.37)			
		23)1.75(0.28)			
		24)1.60(0.32)			
		25)1.72(0.24)			
		26)2.42(0.24)			
		27)2.14(0.23)			
8.21(0.21)	8.21(0.21)	28)2.03(0.25)		29i)2.58(0.20)	
		29)2.62(0.30)		29ii)1.64(0.51)	
		30)2.21(0.20)			
		31)1.75(0.25)			
		32)1.74(0.47)			
		33)1.89(0.25)			
		34)1.41(0.18)			
		35)1.77(0.43)			
		36)1.83(0.38)			
		37)1.75(0.15)			
		38)1.43(0.18)			
		39)1.18(0.20)			
		40)1.08(0.08)			
		41)1.11(0.22)			
		42)1.29(0.28)			
		43)1.02(0.29)			
		44)1.11(0.22)			
		45)1.11(0.14)			
		46)1.03(0.20)			
		47)1.15(0.21)			
		48)0.85(0.32)			
		49)0.76(0.14)			
		50)0.81(0.23)			
		51)0.80(0.23)			
		52)0.71(0.28)			
		53)0.99(0.13)			
		54)0.64(0.40)		62Ai)2.92(0.46)	
		55)0.64(0.25)		62Aii)3.23(0.24)	
		56)0.49(0.09)		62Aiii)1.90(0.22)	
		57)0.67(0.30)		62Aiv)2.36(0.24)	
		58)0.57(0.21)		62Av)1.28(0.32)	
		59)0.54(0.08)	62A)5.03(0.30)		
		60)0.65(0.39)	62B)2.73(0.22)		
		61)0.43(0.32)	62C)2.03(0.16)	62Bi)2.47(0.36)	
		62)5.66(0.26)	62D)2.18(0.18)	62Bii)1.62(0.38)	
			62E)1.37(0.22)		
			62F)0.62(0.18)		
		63)3.05(0.61)	63A)3.25(0.48)		
			63B)2.01(0.21)		
			63C)1.15(0.17)		
			64A)2.71(0.41)		
		64)2.90(0.45)	64B)1.03(0.29)		
			64C)0.35(0.53)		
		65)4.12(0.30)	65A)3.15(0.34)		
			65A)3.04(0.17)		

* Nominal Diameter (cm)
** Corey Shape Factor

hydration causes the majority of size diminution of these shales and that shape is not radically altered through this process. The shape factor indicates that the fragments are less plate-like than the average shape of bedload samples. This is believed due to the slightly curved nature of the fragments spalled from the cobble, which caused their thickness to be overestimated during measurement.

3.4 Stream Characteristics

3.4.1 Flood Frequency Analysis

Sediment transport formulae require knowledge of the magnitude and frequency of stream flows. When investigating alluvial sediment movement within a region, it is necessary to have flow records for all streams within that region, or estimates of streamflow employing a regional approach. The regional flood frequency approach works on the premise that the pattern of flow will be the same for all streams within a topographically similar region and that basin size is the main determinant of flow magnitudes (Benson, 1950).

Durrant and Blackwell (1959) established flood frequency curves for a number of regions in the Canadian Prairies, based on records of 120 large streams. They, however, advised extreme caution in applying their results to drainage basins smaller than 30 square miles (Durrant and Blackwell, 1959, p. 112). As the majority of watersheds in the Riding Mountain region are smaller than 30 square miles, the flood frequency curve derived by Durrant and Blackwell does not accurately portray the nature of the study area streams. A regional approach cannot, however, be ignored since a high proportion of these streams are not gauged.

A partial, rather than an annual series flood frequency analysis

was undertaken so that those flood events occurring more often than once a year, which could be responsible for sediment movement, would be represented. The stream records from Birnie Creek, Wilson Creek and Scott Creek were used in this analysis. Scott Creek, located outside the main study area, but within the same physiographic zone, was incorporated in the analysis because of the lack of gauged streams within the study area. An annual excedence series and a partial series flood frequency for each stream was constructed using only years of complete summer (April to October) records (after Chow, 1964). The discharge values were standardized into values of discharge per unit area and the curves combined to produce the regional flood frequency curve. The ratio between the maximum daily discharges and maximum instantaneous discharges, where recorded for Wilson and Scott Creeks, was employed to construct flood frequency curves of estimated maximum instantaneous discharges.

3.4.2 Channel Morphology

The stream channel at each of the seventeen sites was surveyed to establish the cross-sectional profile and water surface slope. This aspect was undertaken so that width, depth, cross-sectional area and hydraulic radius could be determined for any depth of flow and utilized in flow equations.

3.5 Flume Experiments

Flume experiments were conducted to determine the empirical relationship between the size of shale particles and the fluid velocity required to initiate movement. Experiments were undertaken at the University of Manitoba, Faculty of Engineering Hydraulic Laboratory. The flume used was 11.5 meters long, 30.7 centimeters wide, with a

maximum depth of 30.0 centimeters. The experimental sediment bed occupied a space one meter long by 6 centimeters deep. Observations were restricted to the central third of the sediment bed to avoid the influence of higher flow velocities associated with the smooth beds upstream, and downstream (Plate 7).

An initial run using a wide variety of grain sizes indicated that movement could be initiated for all but the largest particle sizes. Further trials using homogeneous samples of sieved sediment established the operational method.

During trial runs discrepancies were noted between discharge values calculated using readings from the 'V-notch' weir measuring outflow and the venturimeter measuring inflow. To alleviate this, both were calibrated by using a volumetric tank to measure the discharge over a set period of time (Appendix 2).

For bed samples with a mean size larger than 9.25 millimeters, it was necessary to restrict flow depths to achieve critical erosion velocities. Under these supercritical flow conditions a hydraulic jump formed over the sediment bed whose energy release caused uncontrollable scour (Plate 8). Slope was therefore increased to move the hydraulic jump downstream and produce a smooth though undulating water surface over the sediment bed (Plate 9). The cross-sectional area under these conditions was obtained by averaging the mean depths of flow over active areas of the bed.

Slopes were altered from .008 to .017 during the course of experiments. These values are fairly characteristic of natural conditions where slopes were found to range from .004 to .011.

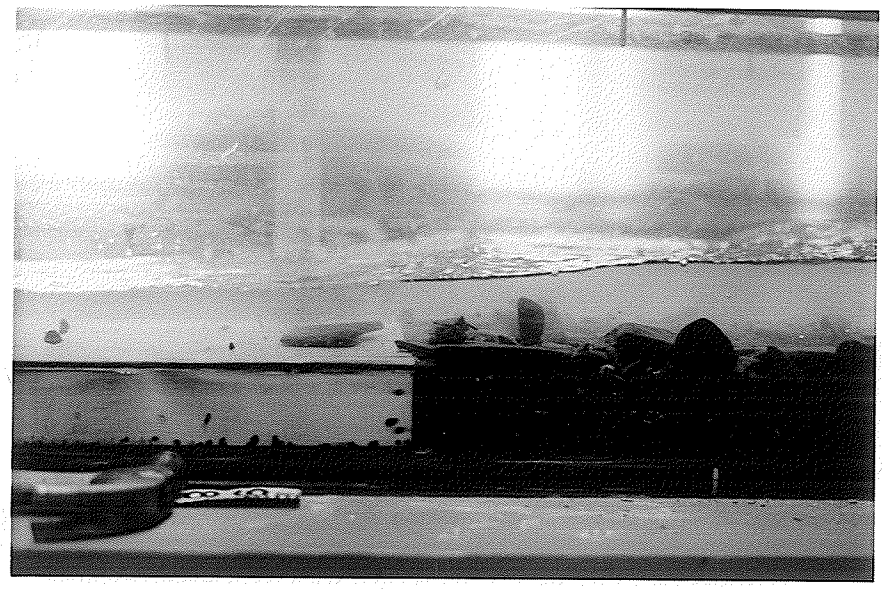

Flow Direction

HIGHER FLOW VELOCITIES OVER THE SMOOTH BED, DOWNSTREAM OF THE SEDIMENT BED

Plate 7.

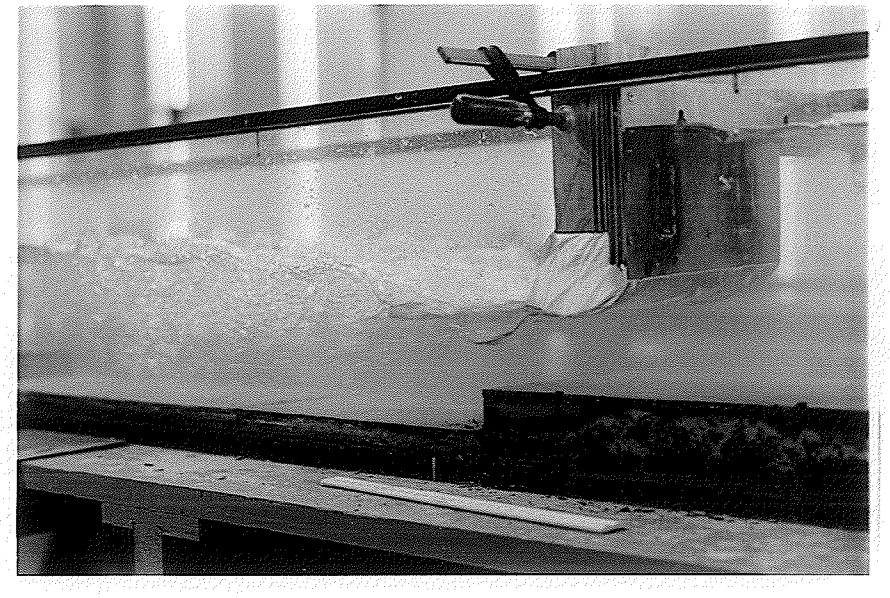

Flow Direction

HYDRAULIC JUMP FORMED UNDER SUPERCRITICAL CONDITIONS

Plate 8.

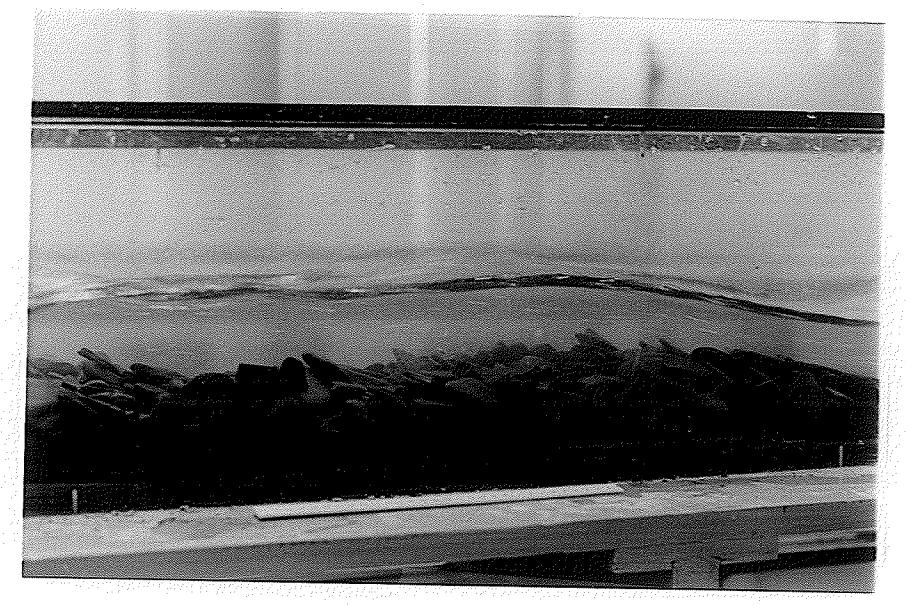

Flow Direction

SMOOTH UNDULATING FLOWS PRODUCED BY INCREASING FLUME SLOPE

Plate 9.

3.6 Summary

Each of the previously discussed procedures provided data which were utilized in estimating the frequency of sediment movement. During the course of flume experiments it had been noted that when 50% of the bed had become mobile, the bed packing arrangement failed and the whole bed became mobile. It was believed that this would also occur in the armour plated beds of the natural streams and thus the D_{50} size was designated as the particle size controlling bed mobilization. This size was determined for each site from the size distributions of the bed load samples. The flume derived critical erosion velocity formula made it possible to calculate the velocity capable of moving the D_{50} rock and, thus, the velocity responsible for bed mobilization. Morphometric measures allowed the Manning equation to be applied and the discharge associated with the critical velocity for a particular site to be calculated. The frequency with which this discharge was reached could then be determined from the regional flood frequency curve.

CHAPTER 4

RESULTS

4.1 Introduction

Estimation of the frequency of stream bed mobilization requires that information about many aspects of the streams be collected and that certain relationships between these characteristics be examined. The data presented thus far has only been concerned with the characteristics of transported material. This chapter will examine the pertinent relationships required for the estimation of the frequency of sediment movement. First of all, it discusses the development of a critical erosion velocity formula for shale particles. An attempt is also made to establish a relationship between basin area and stream discharge by use of a regional flood frequency analysis. Subsequently, the relationships developed are used in conjunction with the Manning equation to estimate the frequency of shale sediment movement in the study watersheds.

4.2 Results of Flume Experiments

Seven separate bed samples were prepared by sieving and categorized according to mean grain size. Trial runs established the operational method employed. A known discharge (Q) was passed through the flume and flow depths gradually decreased until velocities were sufficient to initiate particle movement. Four stages of bed load movement were observed and categorized in accordance with Kramer (1932):

1) the stationary condition;

2) the condition of slight movement of which a countable number of the finest fractions are set in motion;
3) the condition of medium movement in which particles of average size move in quantities no longer countable by observation;
4) the condition of general movement at which stage the largest particles start to move.

The tractive force at which particle motion becomes general (Stage 4) is termed critical by Kramer (Bogardi, 1974, pp. 154-155). Critical erosion velocity (V_{mc}) was operationally defined as the mean cross-sectional velocity (Q/A_x) causing sufficient particle motion that the bed packing arrangement failed and the bed became mobile. This was considered to be equivalent to Kramer's Stage 4. Each particle size category was tested until the repeatability of results gave an acceptable degree of confidence in the data produced.

The results of each run (Table 3) were plotted and the curvilinear relationship between particle size and the critical erosion velocity noted (Figure 12). Subsequently the data were transformed to logarithms and the least squares regression line was calculated to be $V_{mc} = 0.29D_s^{.50}$, where D_s is particle size in mm and V_{mc} is the mean cross-sectional velocity in m/s.

Application of this formula is difficult, however, since sieve diameter most closely approximates the b-axis of non-spheroidal grains (Blatt, Middleton, and Murray, 1972, p. 47) and bed load grain size distributions were constructed using nominal diameter, the formula was computed using the nominal diameter equivalents of the b-axial values (Figure 13). It had been determined during the course of bed load sampling that the relative axial lengths of the average shale particle were 1.48, 1.0, and .26 for the a, b and c planes, respectively.

TABLE 3

PARAMETERS OBSERVED TO CALCULATE CRITICAL EROSION VELOCITY (V_{mc})

Mean Particle Size (mm) D	Discharge (m^3/s) Q	Critical Water Depth (mm) Dc	Flume Slope %	Cross Sectional (Area (mm^2) AX	Mean Velocity (m/s) Q/AX = V_{mc}	Average V_{mc}
2.4	0.021	151		47867	0.439	
2.4	0.021	152		48184	0.436	
2.4	0.021	152	0.06	48184	0.436	.44
2.4	0.015	107		33919	0.442	
3.42	0.023	132		41844	0.550	
3.42	0.022	134		42478	0.518	
3.42	0.023	134	0.06	42478	0.541	.54
3.42	0.023	138		43746	0.532	
3.42	0.024	137		43429	0.543	
3.42	0.024	141		44697	0.539	
3.42	0.024	141		44697	0.539	
5.15	0.027	122		38674	0.698	
5.15	0.024	109		34553	0.690	
5.15	0.024	108	0.06	34236	0.701	.69
5.15	0.024	109		34553	0.690	
9.25	0.030	108		34236	0.876	
9.25	0.030	107	0.06	33919	0.884	.88
15.75	0.030	85		26945	1.113	
15.75	0.030	84	0.12	26628	1.127	1.13
15.75	0.030	83		26311	1.140	
15.75	0.030	84		26628	1.127	
22.2	0.030	* 72		22824	1.314	
22.2	0.030	* 70		22190	1.352	
22.2	0.030	* 68	0.175	21556	1.392	1.35
22.2	0.030	* 69.6		22063	1.360	
31.45	0.030	* 57.5		18228	1.646	
31.45	0.030	* 60	0.175	19020	1.577	1.62
31.45	0.030	* 58		18386	1.632	

*Avg. depth of flow over the bed.

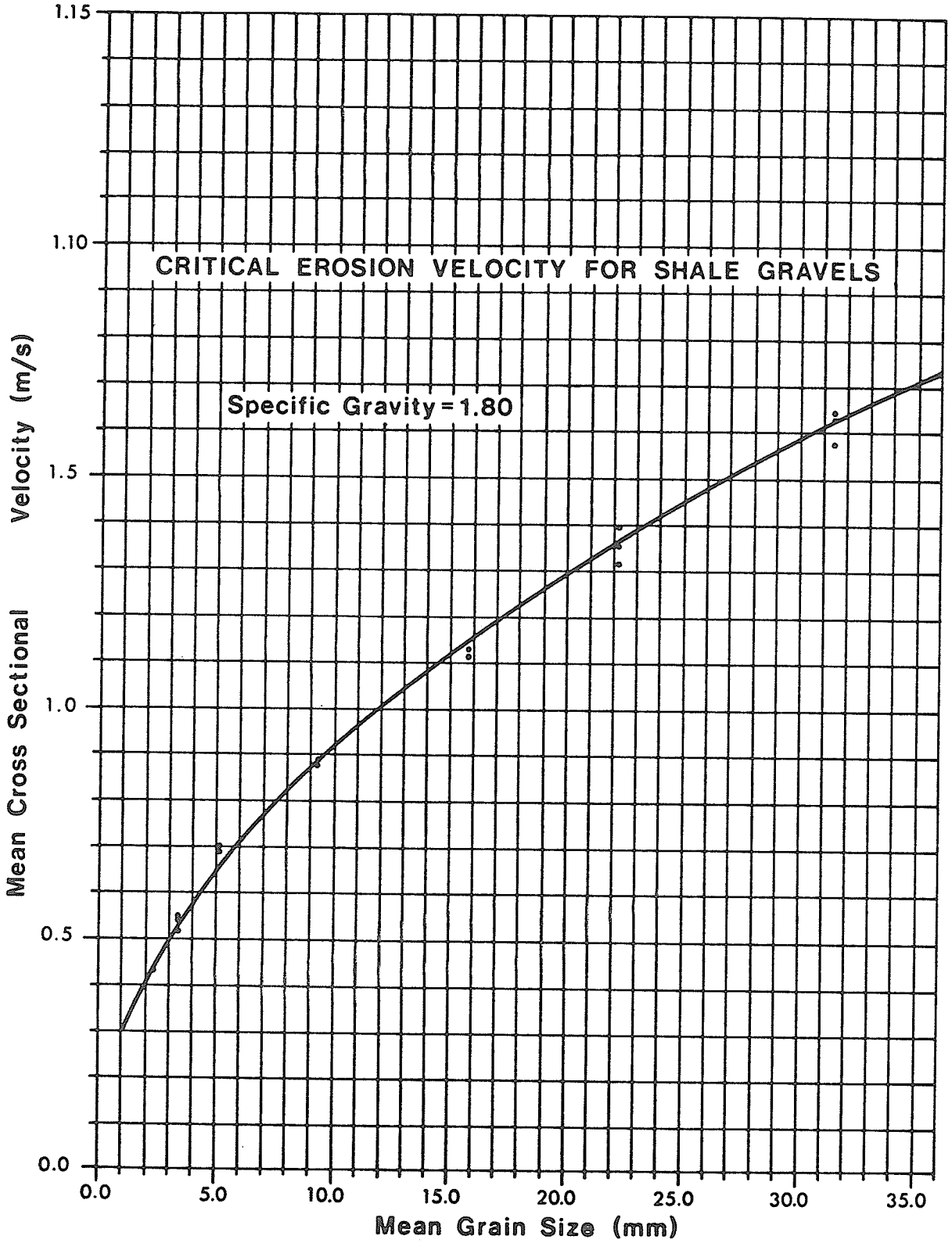
CRITICAL EROSION VELOCITY FOR SHALE GRAVELS
Specific Gravity = 1.80
Mean Cross Sectional Velocity (m/s)
Mean Grain Size (mm)
1.15
1.10
1.5
1.0
0.5
0.0
0.0
5.0
10.0
15.0
20.0
25.0
30.0
35.0

Figure 12.

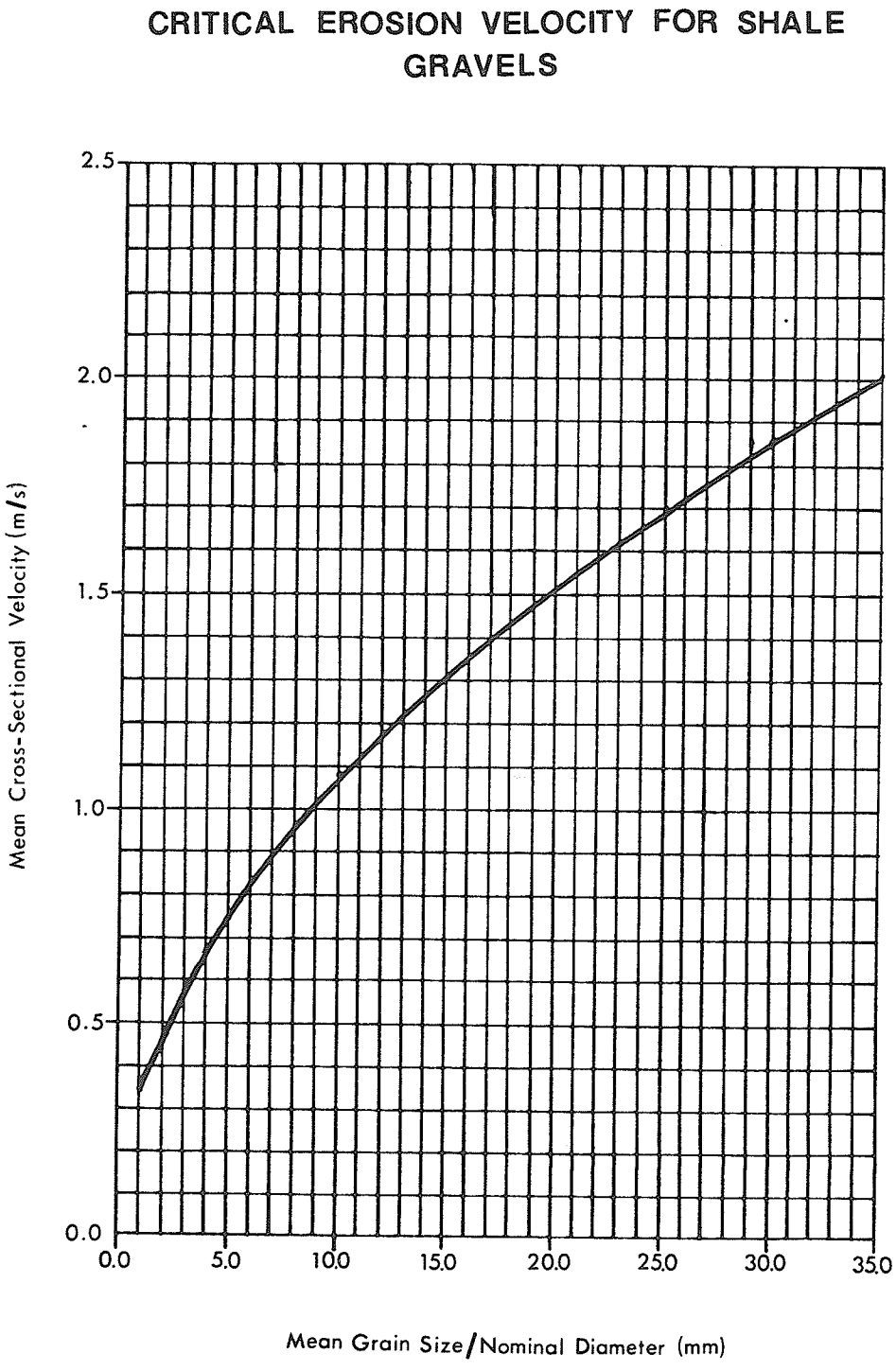
CRITICAL EROSION VELOCITY FOR SHALE GRAVELS
Mean Cross-Sectional Velocity (m/s)
2.5
2.0
1.5
1.0
0.5
0.0
0.0
5.0
10.0
15.0
20.0
25.0
30.0
35.0
Mean Grain Size/Nominal Diameter (mm)

Figure 13.

Thus a particle with a b-axis of 1.0 mm would have a nominal diameter of .725 mm. The formula produced using nominal diameter values was $V_{mc} = 0.34\ D_s^{.50}$. This could be applied directly to the grain size distributions previously constructed and allowed for comparison with incipient motion formulae employing spheroidal grains.

It can be seen from Figure 14 that the erosion velocity function for natural shale gravels is not radically different from those derived by other researchers employing spheroidal material. This high degree of similarity was unexpected due to the low specific gravity of shale (1.8). Bogardi (1974) has demonstrated that low specific gravity sediment (relative to sediment normally used in flume experiment with a specific gravety of 2.65) will have a smaller constant in the erosion velocity function. As the constant in the erosion velocity formula for shale is not lower, another grain characteristic, which is believed to be grain shape, must compensate for the low specific gravity.

Theoretical modelling allows a possible explanation for this apparent paradox to be postulated. Shale, unlike other sediments is thin and platelike and as a result its hydraulic behaviour is markedly different. The movement of spheroidal grains is primarily due to form drag, the reduction in pressure on the lee side of the grains as a result of turbulence. This turbulence will only occur when the increase in boundary layer pressure from the shoulder to the tail of the grain is of sufficient strength to cause a stall in the flow of boundary layer fluid and a reversal in the direction of flow behind the point of stall. An adverse pressure gradient of sufficient strength to cause this stall is unlikely to occur over the surface of the streamlined shale particles. If form drag did develop it is unlikely that it would cause

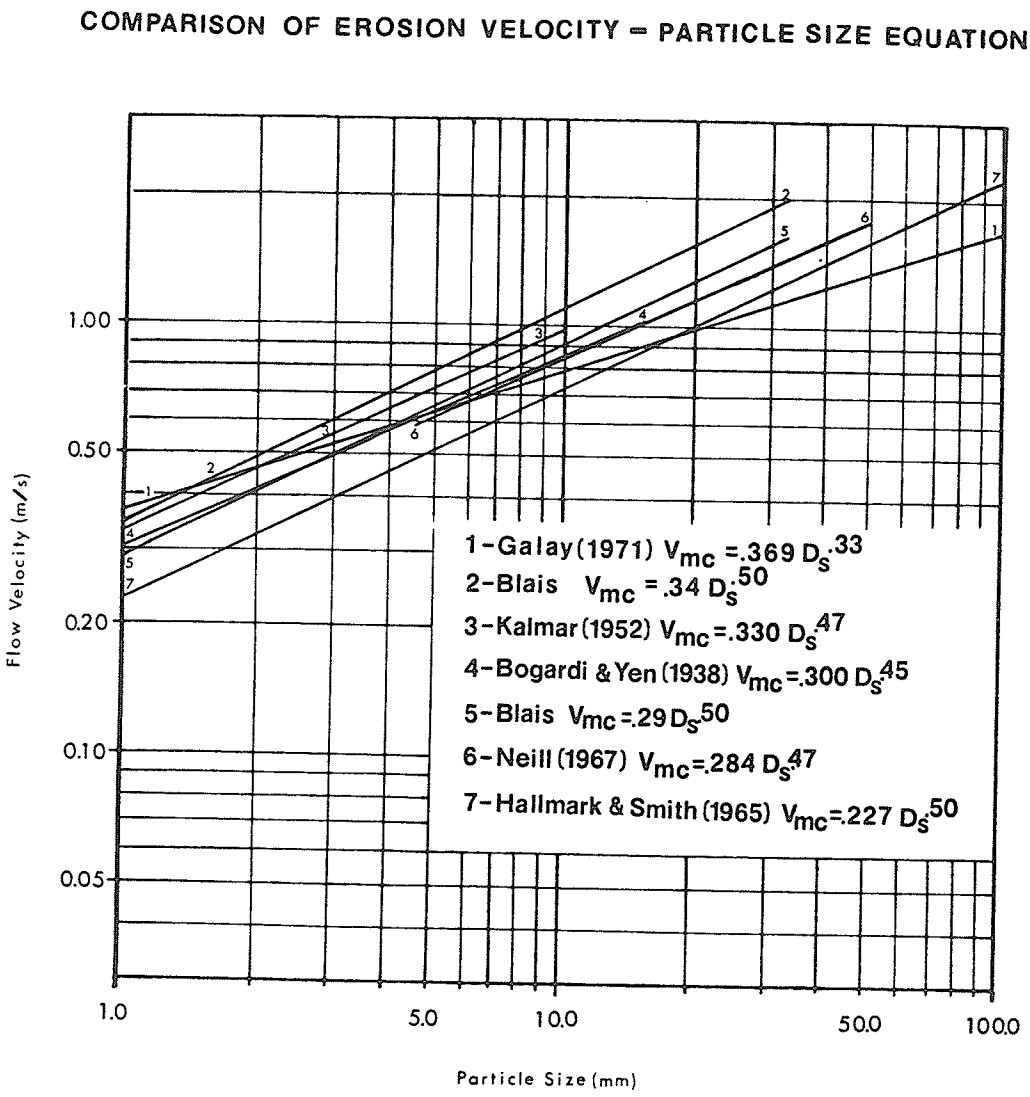
COMPARISON OF EROSION VELOCITY – PARTICLE SIZE EQUATIONS
1.00
0.50
0.20
0.10
0.05
Flow Velocity (m/s)
1.0
5.0
10.0
50.0
100.0
Particle Size (mm)
1-Galay (1971) Vmc =.369 Ds.33
2-Blais Vmc =.34 Ds.50
3-Kalmar (1952) Vmc=.330 Ds.47
4-Bogardi & Yen (1938) Vmc=.300 Ds.45
5-Blais Vmc=.29 Ds.50
6-Neill (1967) Vmc=.284 Ds.47
7-Hallmark & Smith (1965) Vmc=.227 Ds.50

Figure 14.

movement due to the high resistance afforded by the particle's orientation. The action of the drag force due to the shape and imbrication angle (15^{o}) of shale particles would be to pack the particles more securely against the downstream grains (Figure 15).

The same grain characteristics which resist the development of form drag are conducive to generating a lift force. The pressure reduction which results from the fluid accelerating over the shale's upper surface (Figure 16) is enhanced by the large surface area of the particle. When this force is of sufficient strength the grains will rise vertically into the flow (as observed during the course of flume experiments) weakening the bed packing arrangement and ultimately causing bed mobilization. The velocity required for this to occur is similar to that required to move a bed of spheroidal grains which could roll or tumble over the bed.

4.3 Results of Flood Frequency Analysis

The flood frequency analysis was undertaken in hopes of deriving a regional flood frequency curve that could be applied to any basin within the study area. To achieve this, the discharge values for the three streams used to develop the regional curve were reduced to values of discharge per unit area. In this way, the flood frequency curve for any given basin could be derived by multiplying the regional curve by that basin's respective area.

The flood frequency curves for each of the basins examined were computed using the technique outlined in Chow (1964), and return periods were calculated employing Weibull's (1939) formula, $T = \frac{N + 1}{m}$, where N is the total number of events and m is the rank of the event to be plotted. All events of a magnitude greater than the smallest annual

Fluid Forces Acting on an Imbricated Bed Under Turbulent Flow Conditions

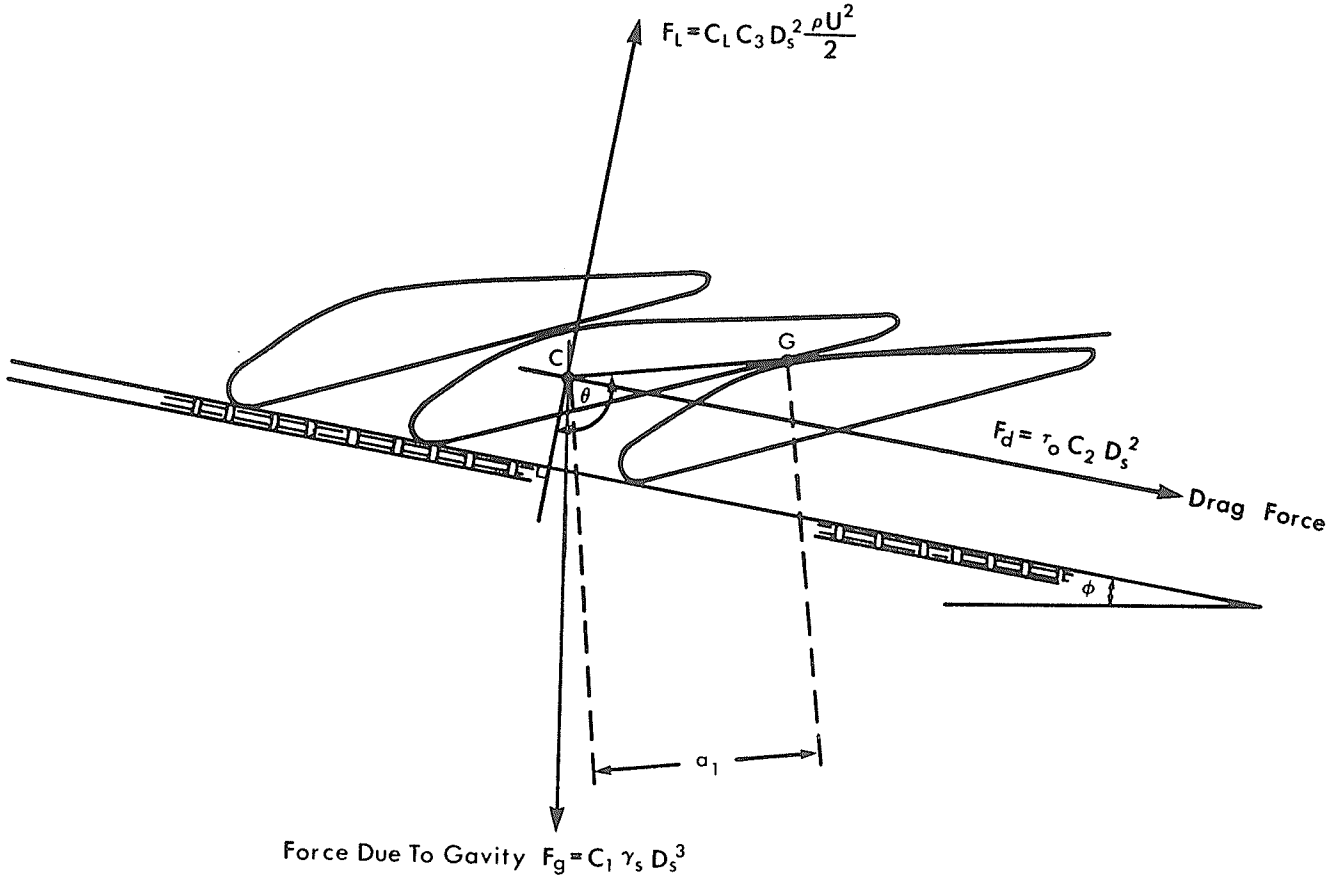

Figure 15.

Theoretical Pressure Distribution Over Shale Particle's Upper Surface
(Viscous Flow at High Reynold's Numbers)

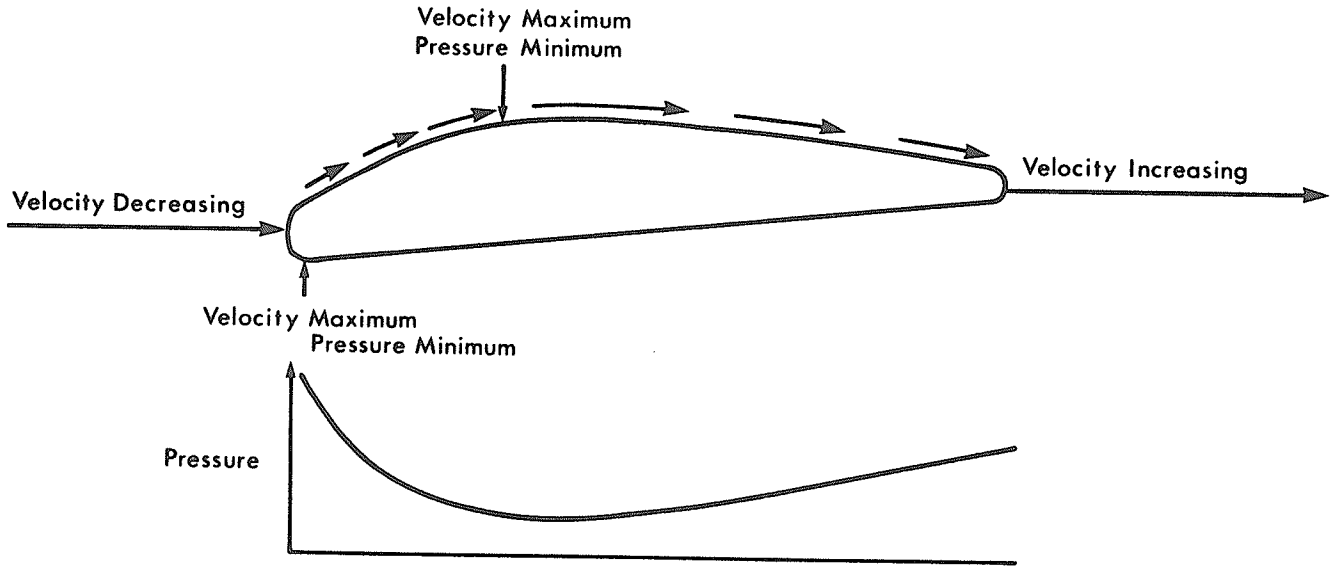

(Adapted From Prandtl and Tietjens, 1934)

Figure 16.

peak flow during the length of record, were plotted in the partial series analysis. Once the partial series (with recurrence intervals in events) and the annual excedence series (with recurrence intervals in years) had been plotted for each stream (Figures 17 and 18 respectively), regional flood frequency curves (Figures 19 and 20) were established by averaging the individual curves into a single regional curve. As it is the peak flow event which would be responsible for sediment movement, it was necessary to estimate, in some manner, the peak instantaneous discharges associated with the mean daily discharges used in constructing the flood frequency curves. This was achieved by comparing the peak instantaneous flows associated with annual peak daily discharges for Wilson and Scott Creeks. The other study basin, Birnie Creek, has an insufficient length of record for this analysis. The average ratio derived was used to construct a regional flood frequency curve of estimated peak instantaneous flows (Figures 19 and 20). A further check on the representativeness of this ratio was made by examining the discharge records for all storms resulting in a discharge of greater than 50 cfs on Wilson Creek. The ratio derived by this analysis was the same as that produced when only the annual peaks were considered.

4.4 Stream Channel Morphology

Stream cross-sections for the seventeen surveyed sites are shown in Figures 21 to 23. The water surface slope at each of these sites was established by averaging the surveyed slope along a reach extending upstream and downstream of the study site. As it was not possible to establish the water surface slope during the time of bed mobilization this was assumed to be equal to the slope at low water levels. Such an assumption has been followed in the past by previous researchers

PARTIAL DURATION SERIES FLOOD FREQUENCY CURVES

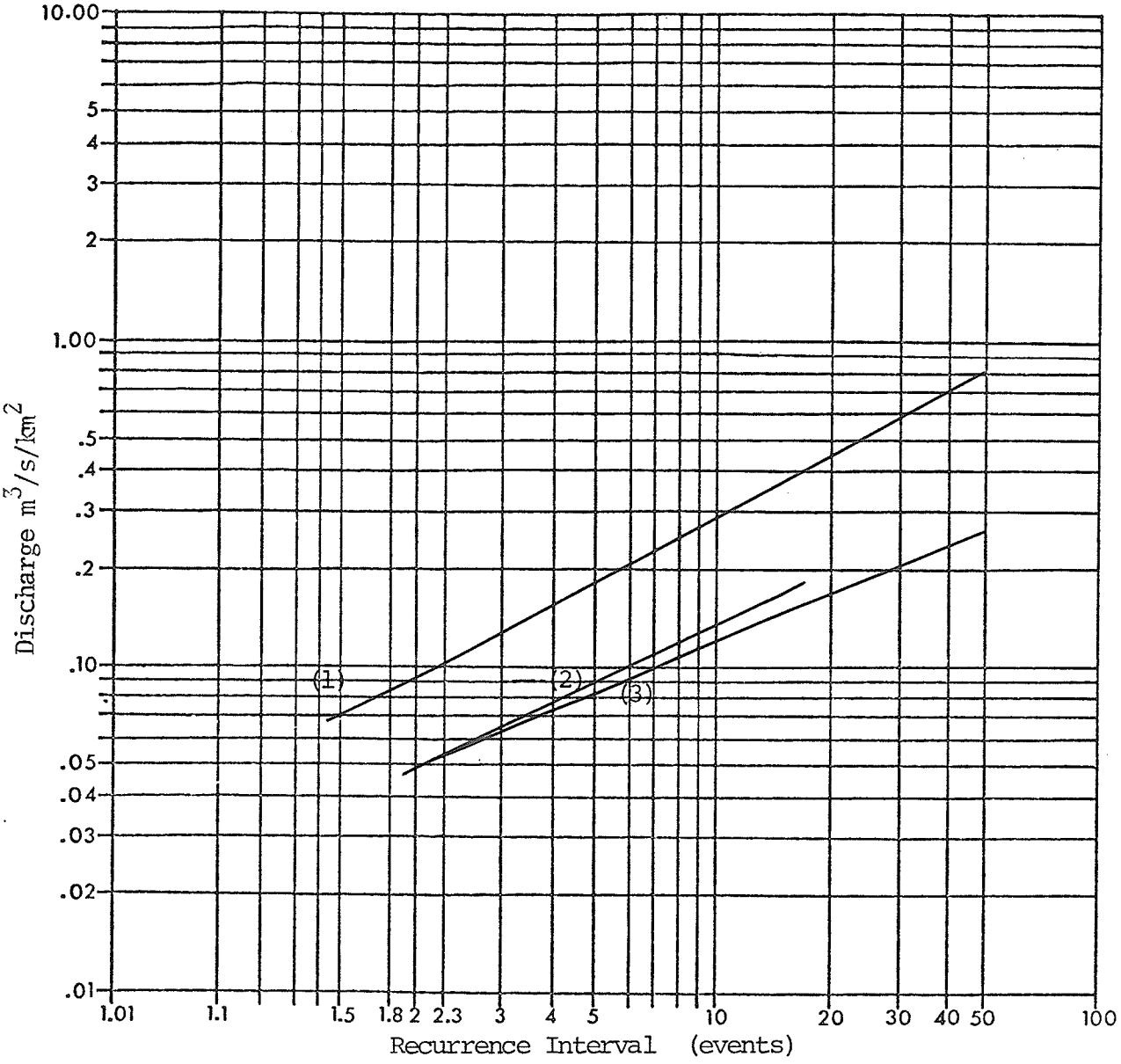

(1) Wilson
(2) Birnie
(3) Scott

Figure 17.

ANNUAL EXCEDENCE SERIES FLOOD FREQUENCY CURVES

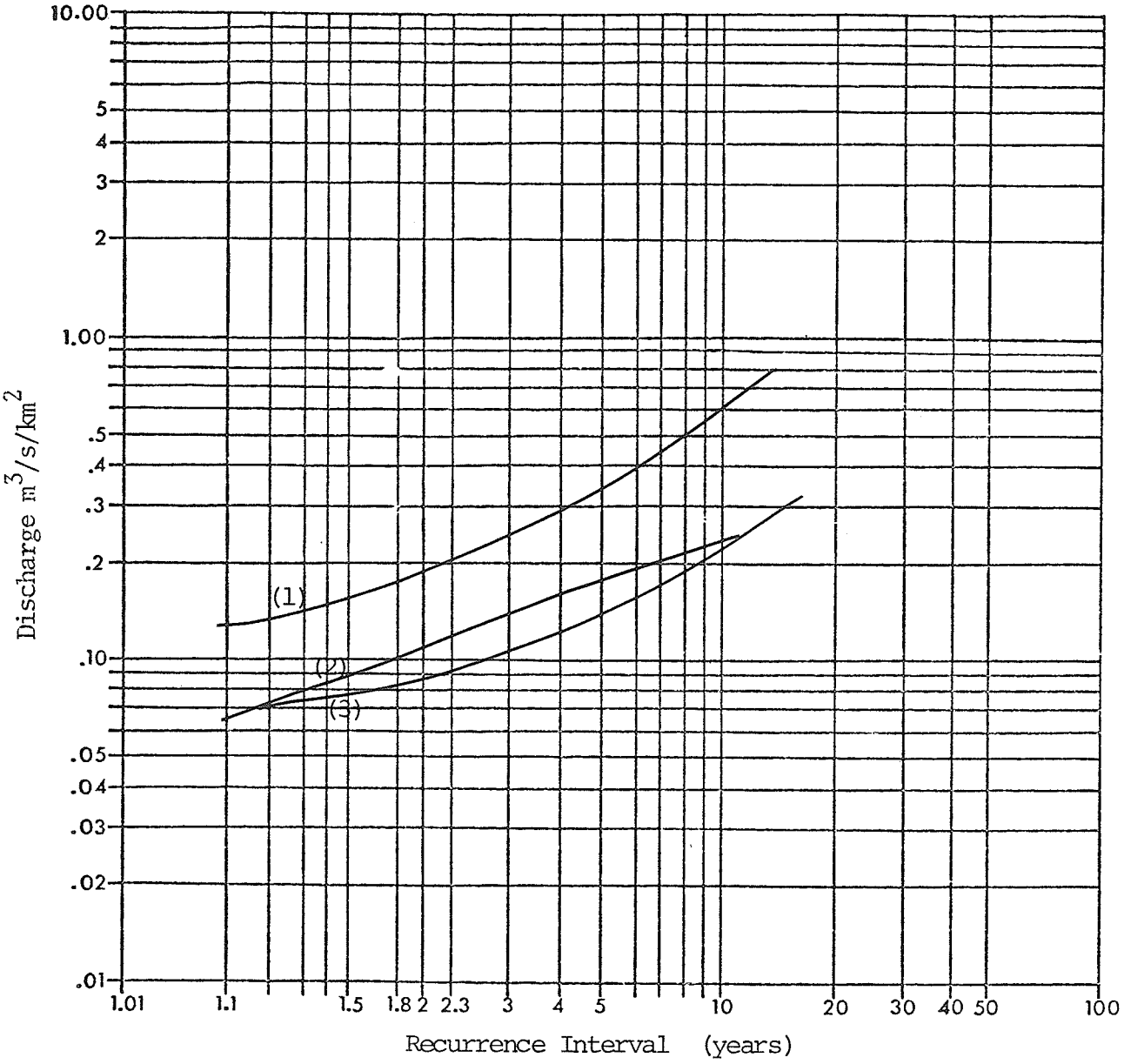

(1) Wilson Creek
(2) Birnie Creek
(3) Scott Creek

Figure 18.

PARTIAL DURATION SERIES REGIONAL FLOOD FREQUENCY CURVES

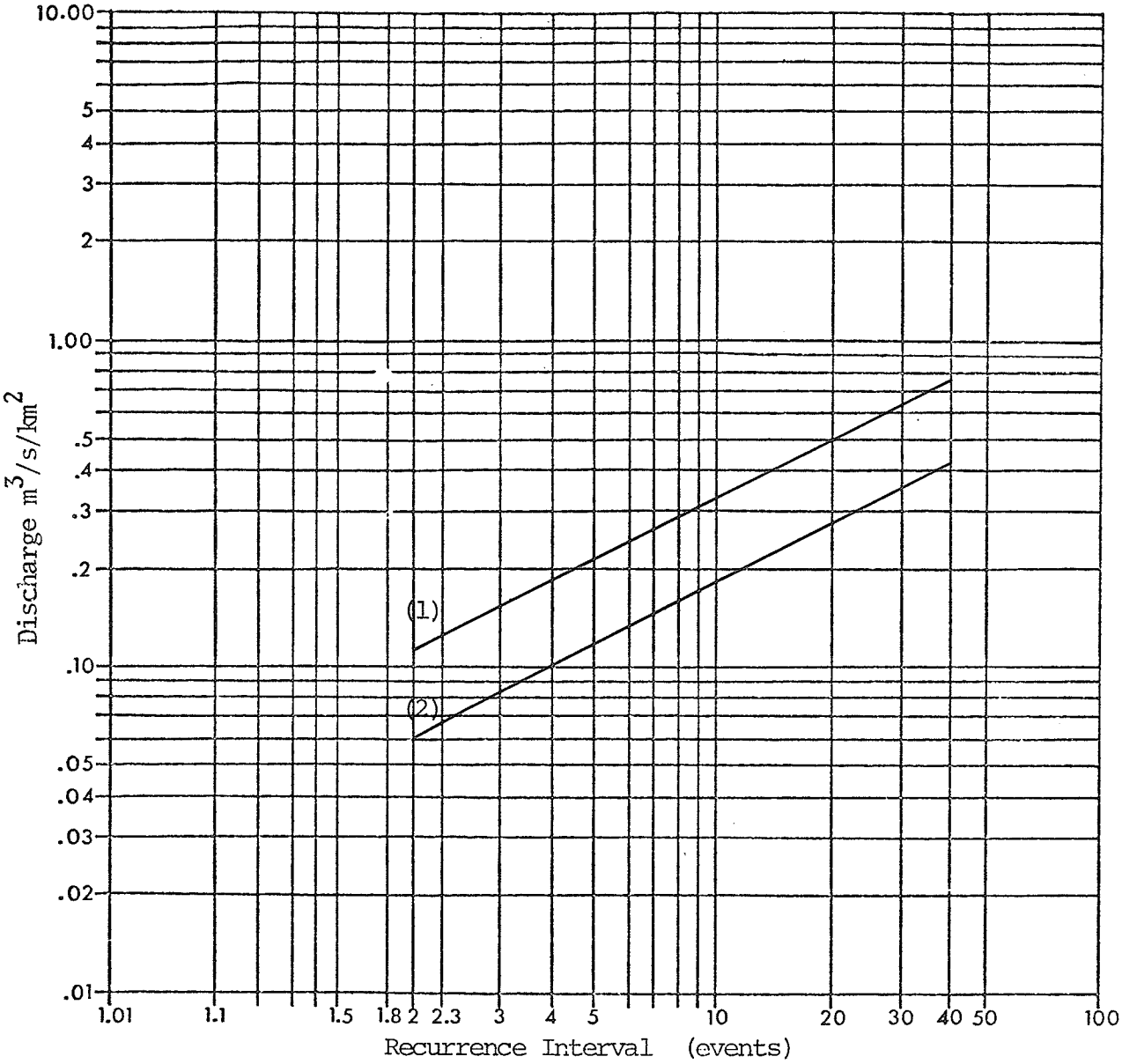

(1) Maximum Instantaneous Discharge
(2) Maximum Daily Discharge

Figure 19.

ANNUAL EXCEDENCE SERIES REGIONAL FLOOD FREQUENCY CURVES

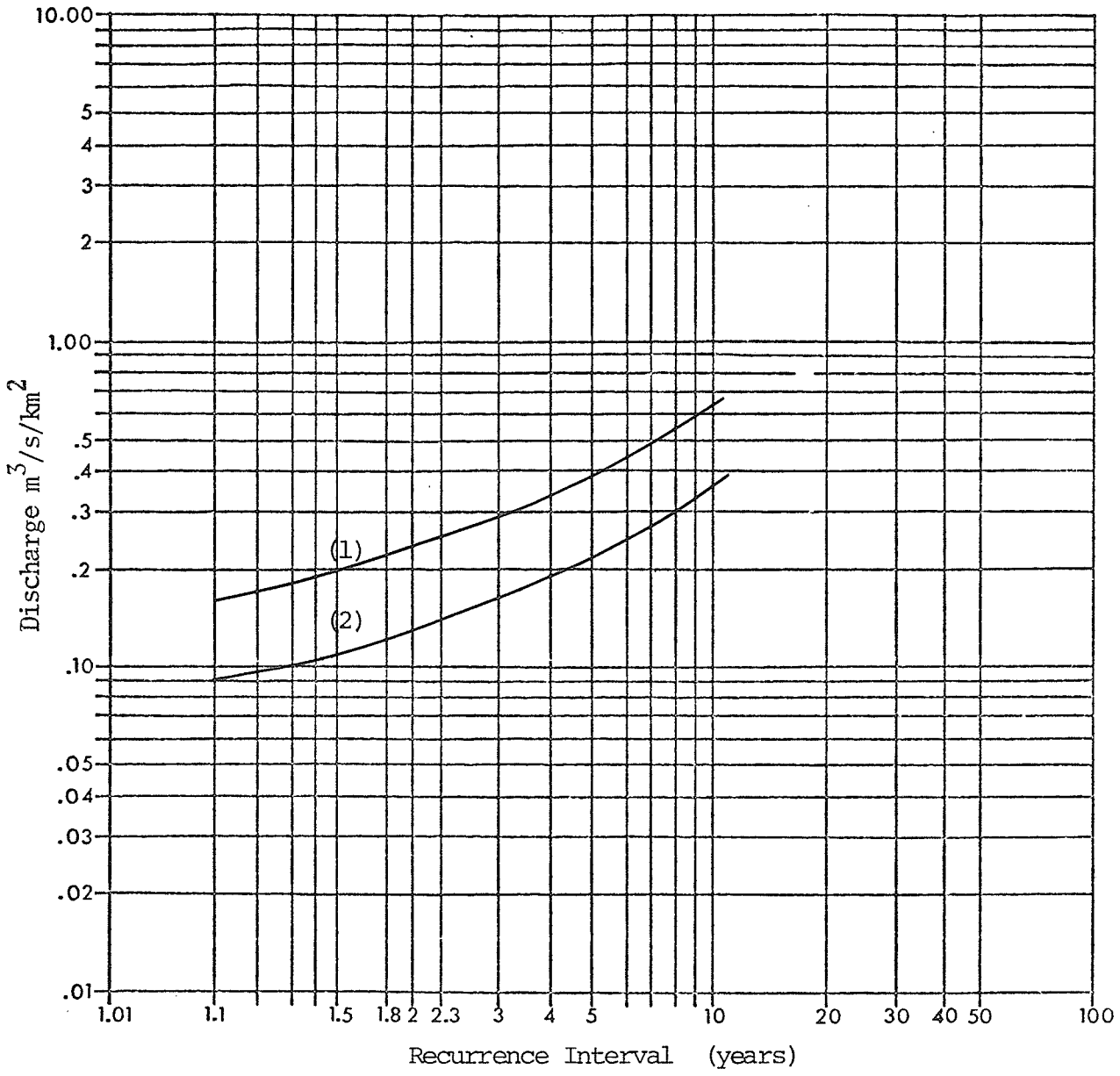

(1) Maximum Instantaneous Discharge
(2) Maximum Daily Discharge

Figure 20.

EDEN CREEK CROSS SECTIONS

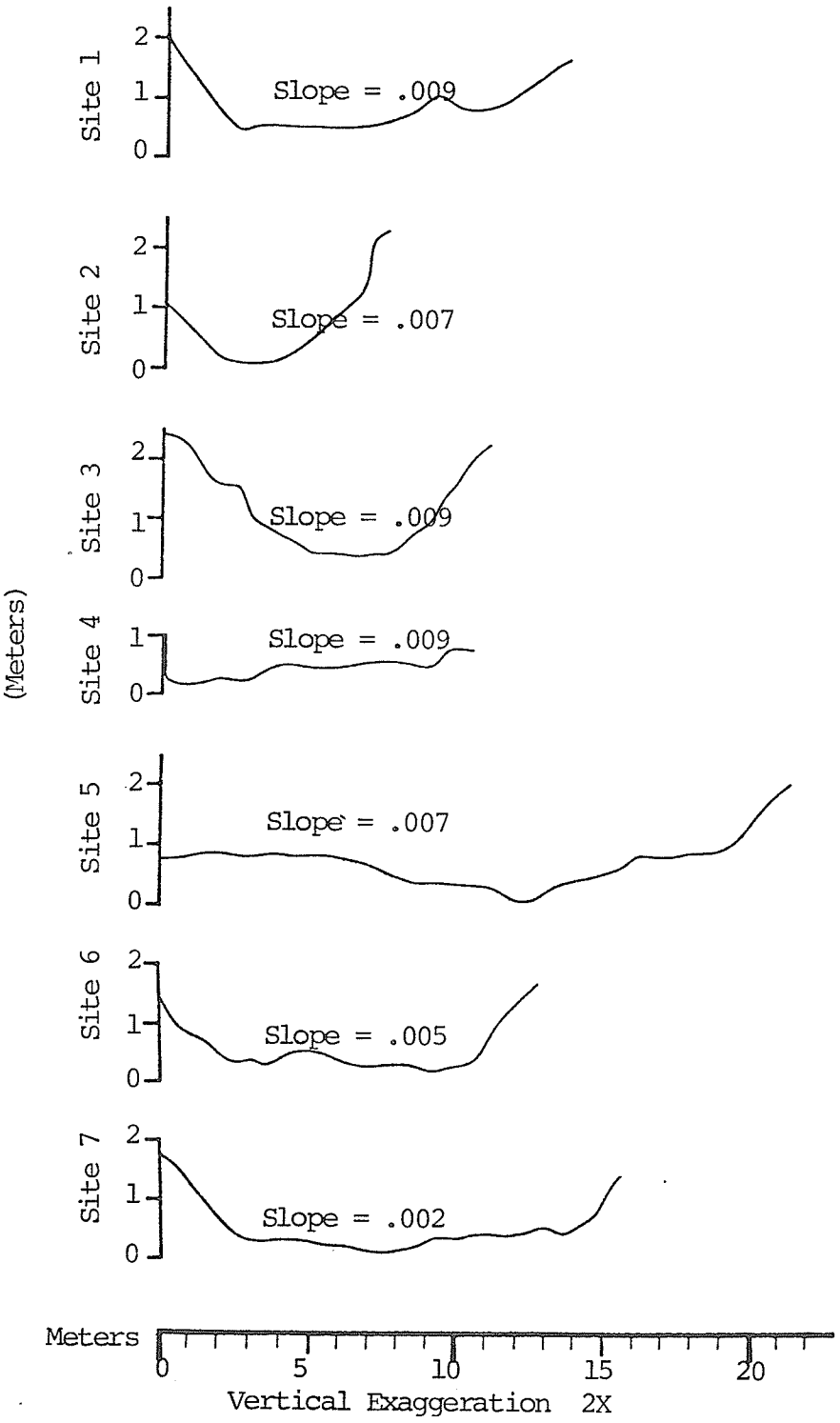

Figure 21.

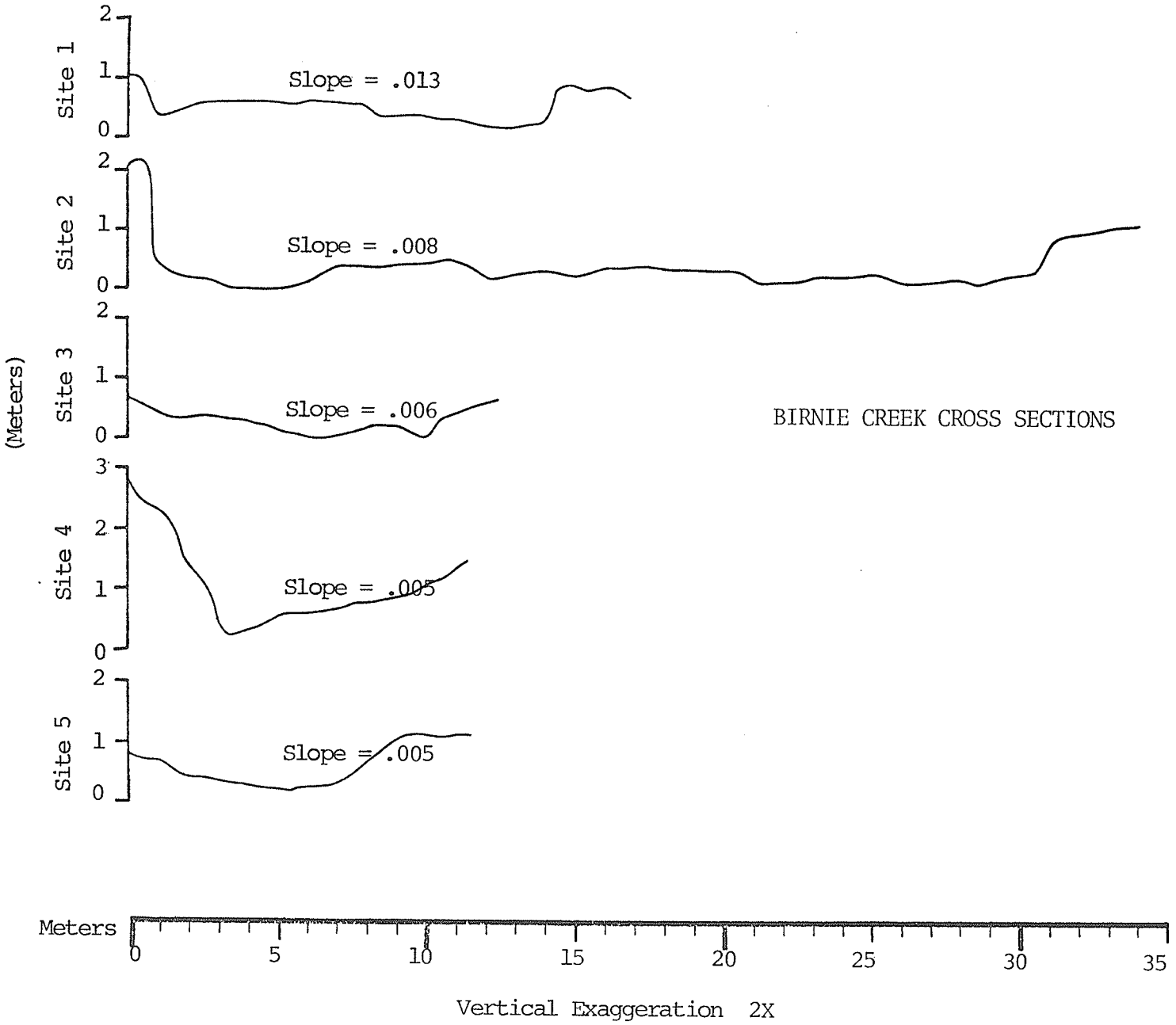
(Meters)
Site 1
Slope = .013
Site 2
Slope = .008
Site 3
Slope = .006
Site 4
Slope = .005
Site 5
Slope = .005
BIRNIE CREEK CROSS SECTIONS
Meters
0
5
10
15
20
25
30
35
Vertical Exaggeration 2X

Figure 22.

WILSON CREEK CROSS SECTIONS

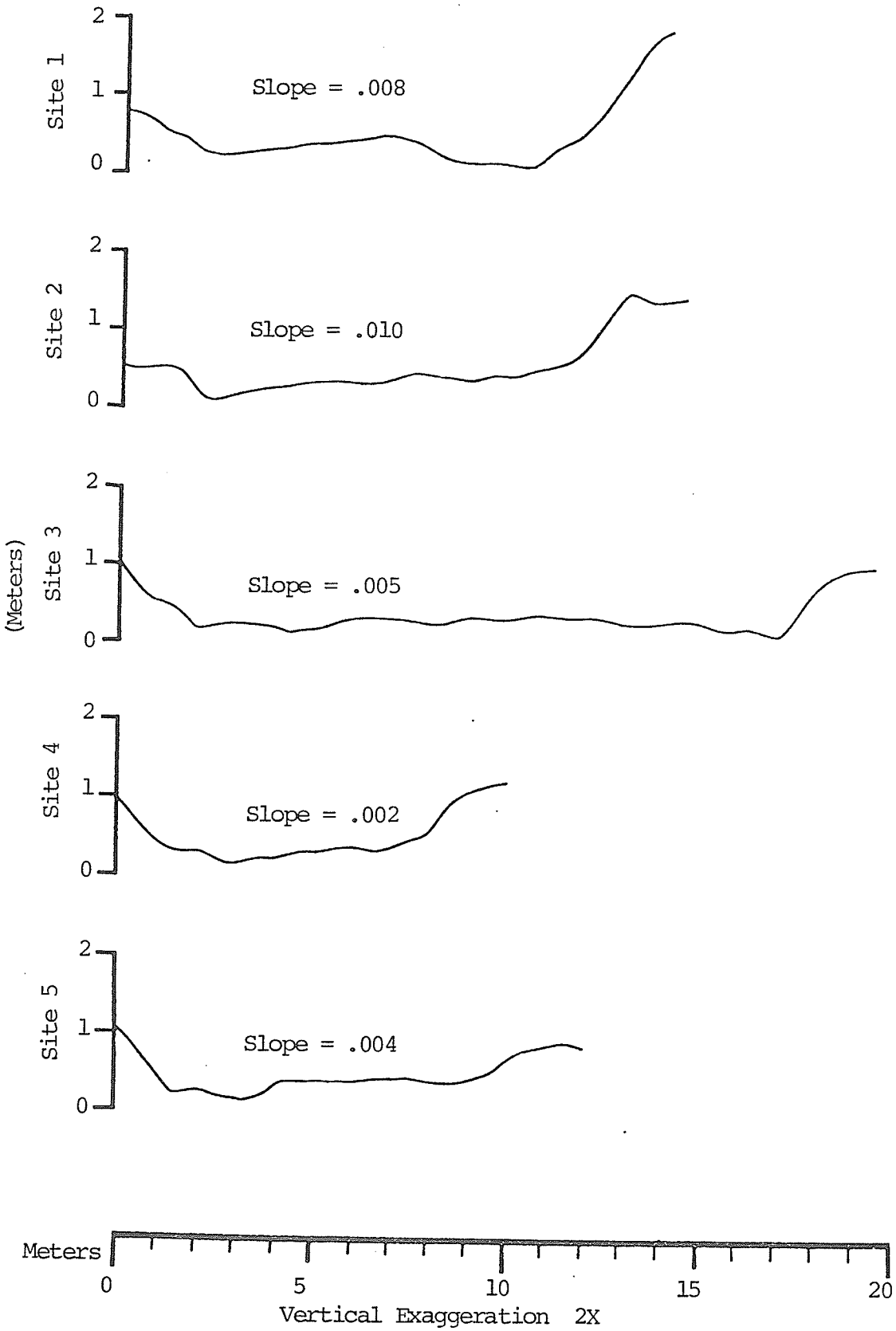

Figure 23.

(e.g. Wolman, 1955).

4.5 Selection of Sampling Sites

One site on each of the three study streams was chosen to estimate the frequency of sediment movement. In order to ensure the comparability of results each was located as closely as possible to the fan apex, at a site demonstrating a minimum of human interference. These sites are designated as Site Number 2 on Eden Creek, Site Number 2 on Birnie Creek and Site Number 1 on Wilson Creek in Figure 3.

4.6 Rationale for the Operational Method Employed to Calculate the Frequency of Sediment Movement

The use of a regional approach to analyze the frequency of sediment movement requires that assumptions be made about stream discharges and the relationship between particle size and flood magnitude. A similarity has been demonstrated between the frequency of discharges per unit area for the three basins used in constructing the regional flood frequency (Figures 17 and 18). It was assumed that the flood frequency curve for the ungauged Eden Creek would be similar to the regional flood frequency (Figures 19 and 20). As the morphological conditions (slope and channel shape) at each of the fan apex sites also reveal a high degree of similitude, the variance in particle size between these sites should reflect the differences in flood magnitude produced by each of the different sized basins. Thus the larger basins will produce higher flood magnitudes and will also exhibit larger particle sizes at the fan apex sites. It was further assumed that the frequency with which floods of a magnitude capable of moving the bed sediment would be similar for all three basins.

4.7 Calculation of the Frequency of Sediment Movement

The frequency of bed mobilization was estimated using a stepwise procedure employing data produced by the previously discussed studies. Knowledge of the average particle size at each site, as determined from the three bed load samples, allowed for calculation of the critical erosion velocity by applying the flume established relationship, $V_{mc} = 0.34D_s^{.50}$. The Manning equation, $U = \frac{R^{\frac{1}{3}}S^{\frac{1}{2}}}{n}$ normally employed to calculate the mean water velocity, provided estimates of the critical hydraulic radius (R). Since the required velocity had been computed, Manning's equation was transposed into the form, $R = (\frac{n\ U}{\sqrt{S}})^{1.5}$ where n is Manning's roughness coefficient, U is average water velocity and s is the slope of the water surface. The roughness coefficient was determined by the formula $n = .038\ D_{75}^{.17}$ (Henderson, 1966, p. 99). The diameter (d) normally used is that of the D_{75} grain size. Due to the flatness of the shales and their tendency to imbricate, the height the D_{75} roughness elements extend from the bed was considered to be, not their diameter, but their thickness (c) (Figure 24). Water surface slope had been determined during the course of site surveys. The required data for these calculations and results are presented in Table 4.

TABLE 4

HYDRAULIC RADIUS CALCULATIONS - REQUIRED DATA AND RESULTS

	d_{50} (nominal diameter cm)	V_{mc} m/s	Water Surface Slope	C_{75} (cm)	n	R_m (m)
Wilson	2.45	1.68	.008	1.16	.018	0.20
Birnie	2.87	1.82	.0075	1.31	.018	0.23
Eden	1.57	1.35	.0075	0.75	.017	0.14

HEIGHT OF SHALE ROUGHNESS ELEMENTS

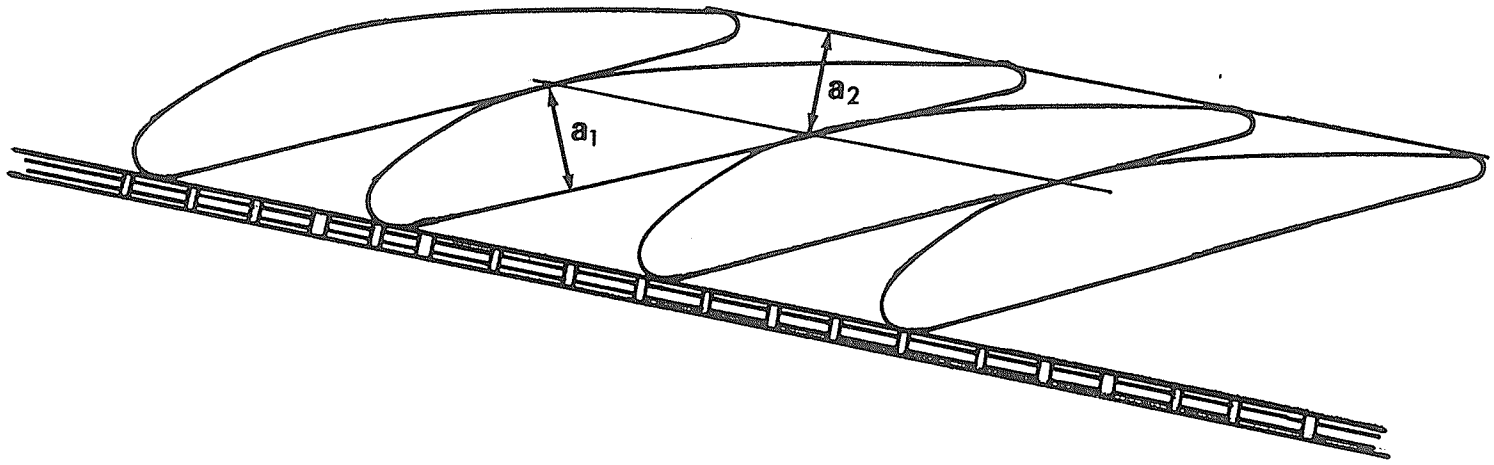

$$a_1 \approx a_2$$

Figure 24.

At this point it became necessary to determine the flow discharge which would produce the required hydraulic radius (R_m), as calculated by the Manning equation. To do this, some estimate of the cross-sectional area of flow under critical conditions had to be made. This could be achieved in two ways. The first method equates the hydraulic radius to the mean depth of flow, an assumption made by previous research on wide channels (e.g. Kellerhals, 1967). The cross-sectional area of flow in this case would be the mean depth multiplied by the top width of the stream. The second technique involves using a sectional method (Gregory and Walling, 1973; p. 131-132) whereby the wetted perimeter (p) and cross-sectional area of flow (A_x) could be determined for any depth of flow (illustrated in Figure 25). Various flow depths were tried until the actual hydraulic radius ($R_s = \frac{A_x}{p}$) closely approximated the required hydraulic radius (R_m) calculated by the Manning equation. This allowed the required discharge ($Q_{crit} = A_x \cdot V_{mc}$) to be determined without making the assumption that mean flow depth is equal to the hydraulic radius.

The critical discharge was divided by basin area so that the frequency of these discharges and thus the frequency of sediment movement could be read directly from the regional flood frequency curve (Figure 20). Table 5 presents the results of this analysis.

THE SECTIONAL METHOD

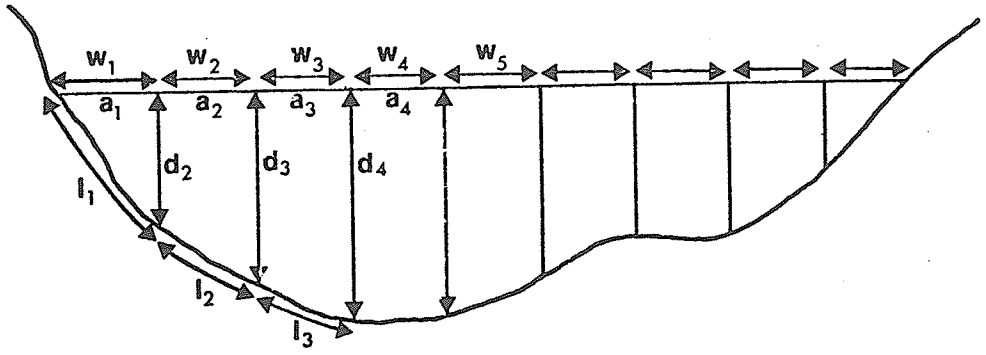

Example Calculations of R for Flow Depth X

1. Divide the cross-section into subsections at appropriate width intervals (approximately 0.5 m)

2. Each subsection has the area:

$$a_i = \frac{d_i + d_{(i+1)}}{2} \cdot w_i$$

3. Total cross-sectional area is:

$$A_X = \Sigma(a_1, a_2, a_3, \ldots a_n)$$

4. The length of the wetted perimeter under each subsection is:

$$l_i = \sqrt{(d_i - d_{(i-1)})^2 + w_i^2}$$

5. The total wetted perimeter is:

$$p = \Sigma(l_1, l_2, l_3, \ldots l_n)$$

6. The hydraulic radius for flow depth X equals:

$$R_S = \frac{A_X}{p}$$

7. The flow discharge associated with this depth is:

$$Q_{crit} = A_X \cdot V_{mc}$$

Figure 25.

TABLE 5

	R_m (m)	D (max. depth of flow) (m)	A_x (m^2)	P (m)	R_s (m)	Q_{crit} (m^3/s)	A (Area) (km^2)	Q/A ($m^3/s/km^2$)	Return Period (Years)
Wilson	.70	.40	2.13	10.64	.20	3.58	22.3	.16	1.1
Birnie	.23	.465	6.54	28.64	.23	11.9	60.68	.20	1.5
Eden	.14	.20	.407	2.80	.14	.55	28.7	.02	unobtainable

The required discharge per unit area for Eden Creek is at variance with those determined for the other two sites. It is believed that this is the result of differences in effective basin area as a percentage of gross topographic area for the three basins. The plateau region has little relative relief and precipitation falling on this area collects into swamps and other low lying pockets of land. These portions of the plateau are non-contributing areas and do not supply discharge waters. It is believed that the Eden Creek basin has a smaller percentage of effective basin area, although this cannot be confirmed from topographic map analysis. Effective basin area is not a consistent or finite value; it is a subjective measure determined by the individual researcher based upon his opinion of the area of the basin contributing to stream flow. This subjectivity alone makes the application of such a value in research difficult, if not questionable. It is the variability in effective basin area which causes it to be inappropriate in the present research. The size of the contributing basin is altered by antecedent moisture conditions, storm intensity and storm duration. Stichling and Blackwell (1957) have demonstrated that effective basin area under dry conditions can be 20% of the contributing area for the

same stream under wet conditions. Between these extremes exists a multitude of possibilities where storage areas either contribute or do not, depending upon storm duration and intensity.

4.8 Stepwise Summary of Procedures Used in Calculating the Frequency of Sediment Movement

1) The critical erosion velocity was determined from flume experiments as:

$$V_{mc} = 0.34\ D_{s_{50}}^{.50}$$

2) The critical hydraulic radius was calculated from the Manning equation as:

$$R = \left(\frac{n\ U}{\sqrt{S}}\right)^{1.50}$$

3) The depth of flow and cross-sectional area required to produce the critical hydraulic radius was determined by trial and error employing the sectional method (Figure 25).

4) Once the required cross-sectional area had been determined, it was multiplied by the critical erosion velocity to determine the critical discharge.

$$Q_{crit} = V_{mc} \cdot A_x$$

5) The critical discharge was divided by the total basin area so that the return period could be read directly from the regional flood frequency curves (Figure 19).

4.9 Problems Encountered With the Operational Method of Calculating the Frequency of Sediment Movement

The accuracy with which the critical erosion discharge and its return period can be determined is affected by the assumptions inherent in a regional approach. The critical erosion velocity employed must be considered as only the best estimate of the actual erosion velocity. It has been demonstrated by numerous researchers that flume derived equations do not accurately portray the natural condition, where a variety of grain sizes and bed forms exist. Similarly, the Manning equation only provides an estimate of the hydraulic conditions as the formula cannot account for all factors affecting flow at a specific site. For example, the problem of estimating the resistance coefficient (n), by itself reduces the confidence which can be placed on this equation.

Of the techniques employed, the regional flood frequency has the greatest degree of inherent error. Effective basin is difficult to determine as it is affected by surface and subsurface conditions and is impossible to delineate from topographic maps. Finally, discharge records are often unrepresentative due to bed mobility at the gauging site; high infiltration rates; or artificial controls upstream.

In spite of these factors the regional approach is a necessity where field observation of bed mobilization is not possible and where stream discharge records are not available. Nevertheless, the frequency of sediment movement estimated by the regional approach is as accurate as possible given the data base available.

CHAPTER 5

SUMMARY AND CONCLUSIONS

5.1 Summary and Major Findings

The primary purpose of this study was to determine the frequency of fluvial transport within the shale bedded streams draining the Riding Mountain portion of the Manitoba escarpment.

To achieve this objective three streams, Eden, Birnie and Wilson Creeks, were chosen to represent the region and the frequency of transport within these streams was calculated. It was rationalized that if these frequencies were similar then they would provide a reasonable indicator of the regional fluvial transport frequency.

The procedure for obtaining fluvial transport frequencies for the individual streams involved two steps.

Initially laboratory and field studies were undertaken to provide the necessary sediment and stream channel data to ascertain the magnitude of floods capable of causing bed mobilization. The frequencies with which these critical discharges occur were determined by use of a regional flood frequency curve.

The first step in this process involved bedload sampling at each of the seventeen selected sites. This provided the grain size distributions essential for the application of a critical erosion velocity formula and the sediment shape characteristics. It was found that a typical shale particle has $^{b}/_{a}$ and $^{c}/_{b}$ length ratios of .677 and .257, respectively, and thus is classified as oblate using Zingg's (1935)

descriptive classification. This particle is further characterized by having a Corey shape factor of .20 and a Cailleux flatness index of 4.79. Bedload sampling was conducted three times during the field season in hopes of obtaining evidence of active transport. The results produced were inconclusive.

It was felt that any significant size diminution of the shale sediments found in these creeks could have an effect in decreasing the critical flow velocity required for bed mobilization. As a result a field weathering study was undertaken along Eden Creek to document the rate and amount of particle size decrease attributable to weathering processes. This was unsuccessful due to the lack of variable flows, vegetation encroachment and the absorption of water through the basal surfaces of particles near the stream channel. Although no conclusive evidence was provided by this study obvious signs of weathering were observed along the other creeks. This led to the weathering process being investigated under laboratory conditions where it was found that hydration is the dominant process. Insufficient data was generated, however, for any conclusions to be made about either the rate or terminal grade of the hydration process.

The critical erosion velocity formula for shale was determined by flume experiments and found to be $V_{mc} = 0.29\ D_s^{.50}$, where D is defined as the median size of sieved sediment. The formula was converted so that nominal diameter values could be used and the function became $V_{mc} = 0.34\ D_s^{.50}$. Velocity in both cases is the mean cross-sectional velocity in m/s and particle size is in mm. These formulae are similar to those derived by flume experiments employing spheroidal material of higher specific gravity. It is believed that the shape of

the shale compensates for the effect of low specific gravity and causes the required velocities to be similar.

Finally, surveys conducted at each of the sites provided the water surface slope and channel cross-sectional data required to determine the critical discharges for one similar site on each stream. The critical erosion velocity for each site was calculated using the bedload particle size distributions. A transposition of the Manning equation allowed the hydraulic radius associated with this velocity to be computed and a sectional method was then employed to ascertain the cross-sectional area of flow with the correct hydraulic radius.

The required discharges ($Q_{crit} = A_x \cdot V_{mc}$) are $0.55m^3/s$ for Site Number 2 on Eden Creek, $11.9m^3$ / s for Site Number 2 on Birnie Creek and $2.58m^3$ / s for Site Number 1 on Wilson Creek.

The return period of these discharges, in values of discharge per unit area ($m^3/s/km^2$) were read from the regional flood frequency curve. The required discharge per unit area for Eden Creek was too small for the return period to be read from the regional curve. Although the amount of stream incision evident along this creek may indicate a higher frequency of bed mobilization, the complete drying of the stream channel during the summers of 1978 and 1979 indicated that both the flood magnitude and transport frequency are over-estimated by the regional flood frequency curve.

The calculated frequency of complete bed mobilization is 1.5 years for Birnie Creek and 1.1 years for Wilson Creek. The average, 1.3 years, is believed to be the representative transport frequency for the Riding Mountain area. The regional flood frequency curve incorporated data from Wilson and Birnie Creeks and thus better represented the basin

area - flood magnitude relationships of these streams.

5.2 Problems Encountered and Areas for Further Research

The problems encountered during the course of this study indicate that further research is required before complete understanding of incipient shale particle motion and an accurate estimate of the frequency of bed mobilization for the individual streams draining the eastern slopes of Riding Mountain can be achieved.

The investigation of weathering under field conditions was unsuccessful, although laboratory research has demonstrated that hydration weathering of these sediments can occur at a very rapid rate. In order to achieve a clearer understanding of the sediment complex it is imperative that both the rate and terminal grade of sediment produced by this process be established. In this way a better comprehension of both the sediment production process and the ability of these streams to transport unusually large volumes of sediment will be achieved.

During the course of flume experiments it became evident that critical velocities for the sediment with a mean size greater than 9.25 mm could not be generated without restricting the flow depth upstream. The supercritical shooting flows which resulted made determination of the cross-sectional area of flow difficult and caused some doubt as to the accuracy of the results obtained. The strength of the relationship subsequently demonstrated by the regression curve, however, indicated that flow depths were properly estimated. The repetition of these experiments using a flume of dimensions capable of generating sufficient velocities, without the use of flow restrictions, is urged to confirm this relationship.

Further flume studies are also required to investigate the effect

of various particle shapes on hydraulic behaviour. Specifically, this would produce evidence to confirm or deny the proposed theoretical model for shale particle movement.

Problems associated with making accurate estimates of effective basin area resulted in the regional flood frequency curve being constructed using values of gross basin area. Evidence from Eden Creek indicates that this can cause over-estimation of both the flow magnitude and frequency of movement for some streams. Further investigations into the relationships between basin characteristics and flood magnitudes for this area are necessary before a viable regional flood frequency approach can be implemented.

The final problem encountered was the inability to make field observations of incipient motion due to low flood magnitudes during the study period. Field studies are essential if the validity of the critical erosion velocity function for shale and the critical discharges proposed by this study are to be verified. At the same time, field research would consider the role of bed armouring and variable grain size mixtures in the determination of critical erosion velocities for natural streams.

REFERENCES CITED

Askoy, S., 1973, The influence of the relative depth on the threshold of grain motion: Proceedings, International Symposium on River Mechanics, Bangkok.

Bagnold, R. A., 1954, The physics of wind blown sand and desert dunes: Methuen & Co. Ltd., London, p. 265.

Baker, V. R. and Ritter, D. F., 1975, Competence of rivers to transport coarse bedload material: Geol. Soc. Amer. Bull., v. 86, pp. 975-978.

Benson, M. A., 1950, Use of historical data in flood frequency analysis: Trans. Amer. Geoph. Union, p. 419.

Bhowmik, N. G., and Simons, D. B., 1970, Stabilization of alluvial channel: Chapt. 17, River Mechanics Institute notes, Colorado State University.

Blatt, H., Middleton, G., and Murray, R., 1972, Origin of sedimentory rocks: New Jersey, Prentice Hall, Inc., p. 634.

Bogardi, J., 1974, Sediment transport in alluvial streams: Budapest, Akademia: Kiado, p. 826.

Cailleux, A., 1945, Distinction des galets marines et fluviatiles: Bull. Soc. Geol. France, 5XV, pp. 375-404.

Chepil, W. S., 1961, The use of spheres to measure lift and drag on wind-eroded grains: Soil Sci. Soc. Am. Proc., v. 25, pp. 343-346.

Chow, Ven Te, 1964, Handbook of applied hydrology: McGraw-Hill, Inc., New York, New York.

Coleman, N. L., 1972, The boundary coefficient of a stationary sphere on a boundary of similar spheres: La Houille Blanche, No. 1.

Corey, A. T., 1949, Influence of shape on the fall velocity of sand grains: Unpublished MSc thesis, Colorado Agricultural and Mechanical College, Fort Collins, Colorado.

DuBoys, M. P., 1879, Etudes du Regime et l'Action Exercee par les Eaux sur Lit a Fond de Graviers Indefiment Affouilable: Annales de Ponts et Chausses, Ser. 5, Vol. 18, pp. 141-195.

Durrant, E. F., and Blackwell, S. R., 1959, The magnitude and frequency of floods on the Canadian Prairies: Proceedings of Hydrology Symposium No. 1, Spillway Design Floods, Nat. Res. Council, Ottawa, pp. 101-160.

Flaxman, E. M., et al., 1966, Sedimentation transportation mechanics: Initiation of motion: Journal of Hydraulics Division, A.S.C.E. Vol. 93, no. HY6, pp. 245-257.

Folk, R. L., 1965, Petrology of sedimentary rocks: Hemphill's, Austin, Texas, p. 159.

Galay, V. J., 1971, Some hydraulic characteristics of coarse bed rivers: Unpubl. PHd Thesis, Univ. Alberta, Edmonton, Alberta, p. 140.

Galay, V. J., 1972, River Engineering 23:766: Course notes, University of Manitoba, Dept. of Civil Engineering.

Gessler, J., 1971, The beginning and ceasing of sediment motion: in: River Mechanics, Shen, H. W. (ed.) Fort Collins, Colorado, Chapt. 7.

Gregory, K. J., and Walling, D. E., 1973, Drainage basin form and process, a gemorphological approach: London, E. Arnold, p. 456.

Hallmark, D. E., and Smith, G. L., 1965, Stability of channels by armour-plating: Journal of the Waterways and Harbours Division, A.S.C.E., Vol. 91, No. WW3, proc. Paper 4452, pp. 117-135.

Helley, E. J., 1969, Field measurement of the initiation of particle motion in Blue Creek near Klamath, California: Geological Survey Professional Paper, 152-G, p. 19.

Henderson, F. M., 1966, Open channel flow: New York, Macmillan Publishing Co., Inc., p. 522.

Hjulström, F., 1935, Studies of the morphological activity of rivers as illustrated by the River Fyris: Geol. Instit. Univ. Upsala Bull., v. 25, pp. 221-527.

Hjulström, F., 1939, Transportation of detritus by moving water: in, Recent Marine Sediments: Amer. Assoc. Petrol. Geol., pp. 5-31.

Isbash, S., 1936, Construction of dams by depositing rock in running water: Proc. Second Congress on Large Dams, Washington.

Kalmar, Gy., 1952, A hord alek mozgas kiserleti tanulmany ozasa (Experimental Studies on Sediment Transport): Budapest, AII. sz. Vizepitestoni Tanszek kiserletei. (manuscript), (in Bogardi, 1974).

Keller, E. A., 1970, Bed-load movement experiments: Dry Creek, California, J. Sed. Pet., vol. 40, pp. 1139-1344.

Kellerhals, R., 1967, Stable channels with gravel-paved beds: Proc. Amer. Soc. Civ. Eng., J. Waterways and Harbor Div., v. 93, pp. 63-84.

Kramer, H., 1932, Modellgesch: ebe und Schleppkraft: Preuss. Versuchsanst Wasserbaunnd Schiffban, Heft 9, Berlin.

Kramer, H., Sand mixtures and sand movement in fluvial models: Transactions A.S.C.E., 1935.

Lane, E. W., and Carlson, E. J., 1953, Some factors affecting the stability of canals constructed in coarse granular materials: Proc. Minn. Intern. Hyd. Convention, Sept. 1953.

MacKay, G. H., and Stanton, C. R., 1969, Wilson Creek study, erosion and sedimentation control: Proc. of Hydro. Symp. (4), Ottawa, pp. 41-77.

Neill, C. R., 1967, Mean velocity criterion for scour of coarse uniform bed material: Proceedings, 12th Congress Inter. Assoc. Hydraulic Res., Fort Collins, Colorado, v. 3, pp. 46-54.

Novak, I. D., 1973, Predicting coarse sediment transport: The Hjulström curve revisited: in, Fluvial Geomorphology, Morisawa, M. (ed.), Pub. in Geomorph. S.U.N.Y. Binghamton, New York pp. 13-25.

Prandtl, L., and Tietjens, O. J., 1934, Applied hydro and aeromechanics: McGraw-Hill Inc., New York and London, p. 311.

Rubey, W. W., 1937, The force required to move particles on a stream bed: U. S. Geol. Surv. Prof. Paper 189E, pp. 121-141.

Shapiro, A. H., 1961, Shape and flow: New York, Doubleday and Company, Inc., p. 186.

Shields, A., 1936, Anwedung de Achnlichkeits mechanik und Turbulenz forschung auf die Geschiebewegung: Mitteilung Preussischen Versuchan stalt Wasser, Erd, Schiffbau, Berlin, No. 26, (translation by W. P. Ott and J. C. Van Uchelen, S.C.S. Cooperative Laboratory, California Institute of Technology, Pasadena, California).

Simons, D. B., and Senturk, F., 1976, Sediment transport technology: Colorado, Water Resources Publications, p. 807.

Stichling, W., and Blackwell, S. R., 1957, Drainage area as a hydrologic factor on the glaciated Canadian Prairies: Internat. Union Geod. and Geophys., Internat. Assoc. Scient. Hydrology, General Assembly, Toronto, Vol. 3, pp. 365-378.

Sundborg, A., 1956, The River Klaralven a study of fluvial processes: Geograf. Ann., v. 38, pp. 125-316.

Tu and Ho, 1938, Iowa City, in Bogardi, J. 1974, Sediment transport in alluvial streams: Budapest, Akademia: Kiado, p. 92.

Vanoni, V. A., et al., 1966, Sediment transportation mechanics; Initiation of motion: Proc. A.S.C.E., v. 92 (HY2), pp. 291-313.

Velikanov, M. A., 1948, Dvishenie nanosov (Movement of Sediment): Moscow, Izd. Minrechflota SSSR. (in Bogardi, 1974).

Weibull, W., 1939, A statistical theory of the strength of materials: Ing. Vetenskaps Akad. Handl. (Stockholm), vol. 153, p. 15.

Wentworth C. K., 1923, A field study of the shapes of river pebbles: U. S. Geol. Surv. Bull., v. 730 c, pp. 103-114.

White, C. H., 1940, The equilibrium of grains on the bed of a stream: Proc. Roy. Soc. London, v. 174 A, pp. 322-334.

Wolman, M. G., 1955, The natural channel of Brandywine Creek, Pennsylvania: U. S. Geol. Survey Prof. Paper 271.

Yang, C. T., 1973, Incipient motion and sediment transport: Am. Soc. Civ. Eng. Proc., Jour. Hydraulics Div., v. 99, HY10, pp. 1679-1704.

Zingg, T., 1935, Beitrage zur Schotteranalyse: Schweiz. min pet. Mitt., v. 15, pp. 39-140.

APPENDIX 1
Grain Size and Shape Watfiv Program

```
      $JOB  WATFIV   NOEXT
 1          DIMENSION A(50),B(50),C(50),WORK1(50),WORK2(50),WORK3(50),
           &WORK4(50),WORKX(50),WORKXX(50),RANK(50),VAR4(50),VAR4A(50),
           &R(50),IR(50)
 2          REAL MEAN4,MEAN3,MEAN2,MEAN1,R,IR
 3          READ (5,*)  (A(I),I=1,50)
 4          READ (5,*)  (B(I),I=1,50)
 5          READ (5,*)  (C(I),I=1,50)
 6          WRITE (6,10)  (A(I),B(I),C(I),I=1,50)
 7       10 FORMAT ('0','A(I)=',G14.7, 'B(I)=',G14.7, 'C(I)=',G14.7)
 8          DO 100 I=1,50
 9          WORK1(I)=A(I)*B(I)
      C     WORK1 CONTAINS PRODUCT A TIMES B
10          WORK2(I)=WORK1(I)*C(I)
      C     WORK2 CONTAINS PRODUCT A BY B BY C
11          WORK4(I)=WORK2(I)**.333
      C     WORK4 CONTAINS GEOMETRIC MEAN VALUES
12       100 CONTINUE
13          DO 11 I=1,50
14          R(I)=WORK4(I)
15       11 IR(I)=I
16          CALL VSORTP(R,50,IR)
17          PRINT6,(I,R(I),I,IR(I),I=1,50)
18        6 FORMAT(' SORT(',I2,')=',F11.6,'IR(',I2,')=',G15.7)
19          CALL NMRANK (WORK4,50,.000001,WORKX,WORKXX,RANK,S,T)
20          DO 200 I=1,50
21          WORK2(I)=WORK1(I)**.5
22          WORK3(I)=C(I)/WORK2(I)
      C     WORK3 CONTAINS COREY SHAPE VALUES
23       200 CONTINUE
24          DO 300 I=1,50
25          WORK2(I)=B(I)/A(I)
      C     WORK2 CONTAINS RATIO B OVER A
26       300 CONTINUE
27          DO 400 I=1,50
28          WORK1(I)=C(I)/B(I)
      C     WORK1 CONTAINS RATIO C OVER B
29       400 CONTINUE
30          WRITE (6,50)  (I,WORK4(I),WORK3(I),WORK2(I),WORK1(I),I=1,50)
31        50 FORMAT ('0',' GEOMEAN ',I2,' IS: ',G12.6,  ' COREYSHAPE ',
           &' IS: ',G12.6, ' B/A ', ' IS ; ',G12.6, ' C/B ',' IS: ',G12.6)
32          CALL VABSMF (WORK4,50,1,VSUM4)
33          MEAN4 = VSUM4/50
34          DO 500 I=1,50
35          VAR4(I)=WORK4(I)-MEAN4
36          VAR4A(I)=VAR4(I)**2
37       500 CONTINUE
38          CALL VABSMF (VAR4A,50,1,VSUM4A)
39          STWO = VSUM4A/50
40          SIGMA = STWO**.5
41          WRITE (6,600) VSUM4,MEAN4,STWO,SIGMA
42       600 FORMAT('0',' SUM=',G14.7, ' MEAN=',G14.7, ' VAR=',G14.7,
           & ' SIGMA=',G14.7)
43          CALL VABSMF (WORK3,50,1,VSUM3)
44          MEAN3=VSUM3/50
45          DO 700 I=1,50
46          VAR4(I)=WORK3(I)-MEAN3
47          VAR4A(I)=VAR4(I)**2
48       700 CONTINUE
49          CALL VABSMF (VAR4A,50,1,VSUM4A)
50          STWO = VSUM4A/50
51          SIGMA = STWO**.5
52          WRITE (6,600) VSUM3,MEAN3,STWO,SIGMA
53          CALL VABSMF (WORK2,50,1,VSUM2)
54          MEAN2=VSUM2/50
55          DO 802 I=1,50
56          VAR4(I)=WORK2(I)-MEAN2
57          VAR4A(I)= VAR4(I)**2
58       802 CONTINUE
59          CALL VABSMF (VAR4A,50,1,VSUM4A)
60          STWO=VSUM4A/50
61          SIGMA = STWO**.5
62          WRITE (6,600) VSUM2,MEAN2,STWO,SIGMA
63          CALL VABSMF (WORK1,50,1,VSUM1)
64          MEAN1=VSUM1/50
65          DO 807 I=1,50
66          VAR4(I)=WORK1(I)-MEAN1
67          VAR4A(I)=VAR4(I)**2
68       807 CONTINUE
69          CALL VABSMF (VAR4A,50,1,VSUM4A)
70          STWO = VSUM4A/50
71          SIGMA = STWO**.5
72          WRITE (6,600) VSUM1,MEAN1,STWO,SIGMA
73          WRITE (6,60) (I,RANK(I),I=1,50)
74        60 FORMAT ('0','ELEMENT ', I2 , ' OF RANK IS:',G14.7)
75          RETURN
76          END
```

APPENDIX II

90° V notch Weir Calibration Curve

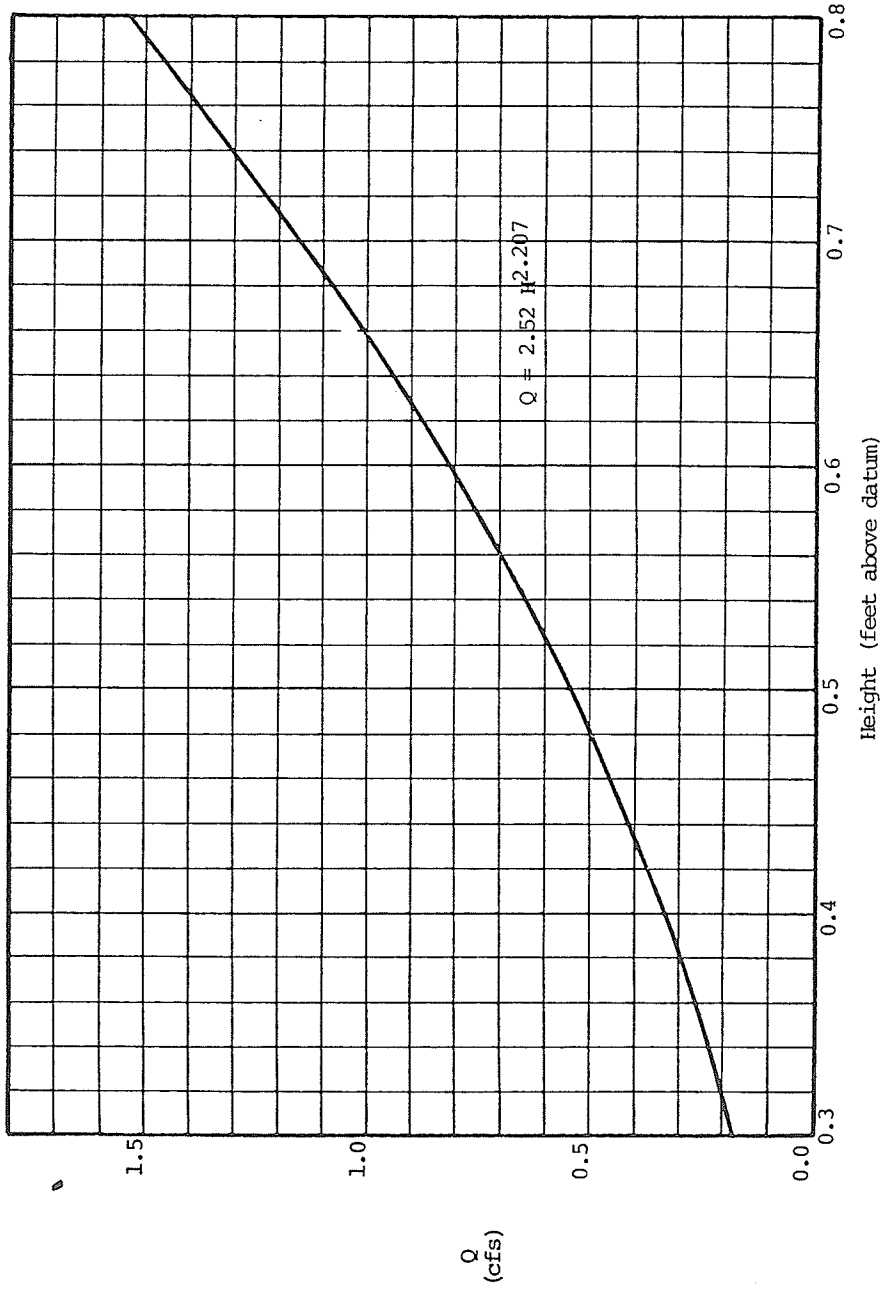

APPENDIX II (con't)

Venturi - Meter Calibration Curve